32AF

THE MEAN FLOW IN ROUND BUBBLE PLUMES

ABSTRACT

Previous experimental studies are reviewed and those whose data are deemed reliable are identified. New experiments at larger scale are described and the results are reported. These are combined with the reliable previous studies to form a data set covering heights from 3.66 to 50 meters and gas flow rates from 0.0002 to 0.59 normal cubic meters per second. This wide ranging data is combined with an integral theory for bubble plumes to determine functional relationships between local plume properties and the entrainment coefficient and the fraction of the momentum flux that is carried in the turbulent velocity fluctuations. These relationships together with the integral theory provide a set of equations that are suitable for numerical solution for the mean flow properties of any round bubble plume. Examples of the numerical solutions are presented and a comparison of one of these with existing experimental data is given.

THE MEAN FLOW IN ROUND BUBBLE PLUMES

by

Jerome H. Milgram

1. INTRODUCTION

When a continuous stream of gas is released in the interior of a liquid the gas takes the form of bubbles which rise due to buoyancy and which impart a generally upward velocity to the surrounding liquid. Such bubble plumes occur above blowouts of subsea gas-containing hydrocarbon wells and it is the desire to understand the hydrodynamics of subsea blowouts that has stimulated the most recent studies of these plumes.

Gas enters the liquid in the form of a jet and the region through which the flow goes from jet-like to plume-like is called the zone of flow establishment. The region of the flow beneath the upper surface of the liquid extending to a depth about equal to the plume diameter is the part of the flow for which the influence of the upper surface is significant and it is called the zone of surface flow. Usually most of the vertical extent of the flow lies in the "pure-plume" region between these two zones. It is called the zone of established flow and is the subject of this paper.

Extensive studies of single-phase plumes have taken place and a thorough review of these is that of Chen and Rodi (1980). The fewer studies of bubble plumes that have been done show that these plumes have both notable similarities and differences with single-phase plumes. This paper extends the integral theory of plumes to include some of these differences and determines approximations for some of the needed functional relationships by analyzing existing small scale data together with new experimental data for plumes of larger scale. A review of important round bubble plume studies known to the author follows. All of the experimental studies have been for air released into water.

Kobus (1968) performed experiments on round bubble plumes in a laboratory basin having a width of 8 m and a depth of 4.7 m with airflow rates up to 0.0058 N m^3/s. For each airflow rate profiles of velocity vs radius were measured and each of these was fit with a gaussian curve whose width and center-line velocity was chosen so as to minimize the error between the curve and the measured data. Kobus found it necessary to average his data over five minute intervals (presumably to obtain reliable results) because the flow was "subject to considerable fluctuations". These fluctuations could have been caused not only by local turbulence, but also by lateral wandering motions of the plume.

If wandering did occur, the long-term time average measurements would show greater widths and smaller centerline velocities than actually existed with respect to the instantaneous locations of the wandering plume centerline; a fact which must be considered in interpreting the data.

Because the air nozzle diameter was very small (0.2 cm in most cases), the flow in the nozzle was subsonic only for airflow rates below 0.0009 N m^3/s. For the higher airflow rates the supercritical flow out of the nozzle could have expanded rapidly to an unknown radius and interacted with the tank bottom so as to add an unknown amount of momentum flux to the plume. Because of this the sonic orifice data will not be considered further here.

Subsonic orifice gaussian fit centerline velocity results were given by Kobus for airflow rates of 0.00040 and 0.00057 N m^3/s. Gaussian fit widths were given for the 0.00040 N m^3/s case, but not at the same set of heights as the velocity data so that interpolation between points is necessary to obtain the centerline velocity-width pairs that are needed for the analysis here. Width data was not given for the 0.00057 N m^3/s case so it can only be approximated by interpolating between the 0.00040 N m^3/s case and the next lowest air flow for which width data is given which is 0.0013 N m^3/s. Due to the uncertainty associated with these steps the Kobus data will not be included here in the primary data set used for determining plume properties. However, these data will be analyzed so they can be compared with other data.

Topham (1975) performed experiments with air bubble plumes in Saanich Inlet off Vancouver Island using air nozzle depths up to 60 m and airflow rates up to 0.66 N m^3/s. Profiles of flow speed vs radius were measured at several heights from a horizontal suspended 12 m long beam which supported 20 vertical current meters. A six minute average of the data from each current meter was used as the velocity at a radius equal to the distance from the beam center to the meter. The results for plume radii and centerline velocities vs height show too many deviations from smooth functions and vary in excessively irregular ways from test-to-test to be suitable for use here in the primary data set. Topham (private communication) has indicated that these matters are related, at least in part, to lateral motions of the beam caused by turbulence in the flow and the fact that the lateral restraint was not stiff. Nevertheless, Topham's measurements are in qualitative agreement with those of similar scale made by the author and which are described subsequently.

Fannelop and Sjoen (1980) conducted experiments in a laboratory basin having a width of 10.5 m and a depth of 10 m using airflow rates up to 0.022 N m^3/s. Fluid velocity at various points was measured and in order to obtain "satisfactory repeatability" they had to average their velocity data over ten minute time intervals. Both the actual data and gaussian curve fits to the profiles of velocity vs radius are presented. The normalized standard deviation for the curve fitting is observed to be about 5%. Details of two different methods for obtaining gaussian curve approximations and their results for these data are described by Sjoen (1982). The standard deviation between results of the two methods is on the order of 4%. For the subsequent analysis and comparisons considered here, the averages of the two sets of results given by Sjoen will be used.

Milgram and Van Houten (1982) performed experiments on bubble plumes in a 1.65 m diameter laboratory tank with a nozzle depth of 3.66 m at air flow rates up to 0.0023 N m^3/s. In addition to measuring profiles of flow speed vs radius at several heights, they also measured profiles of momentum flux and of gas fraction. Observations and measurements of the plumes in the tank showed that plume wandering was sufficient to bias measurements taken as long-term time averages. This difficulty was overcome by the following procedure. When a measurement was to be made at a particular height and radius, three identical measurement transducers were located on a horizontal circle of this radius and concentric with the axis of the tank. The output from each transducer was low-pass filtered with a five second time constant. The resultant signals were processed by an analog-to-digital converter and a digital computer whose program discarded all data except those for which all three signals were equal to within a small fraction of the average signal level. This procedure limited retained data to that for which the plume centerline was nearly centered in the tank so the radius from the instantaneous centerline to the instrument was known. These centering events occurred about once every five minutes on the average. For each transducer location circle, the experiment was continued until eight centering events occurred and the eight measurements were averaged together to obtain the required data point. Profiles of flow speed, momentum flux and gas fraction were fit with gaussian curves with the standard deviation of the fits averaging to about 3% of the centerline values.

All current mean flow theories for bubble plumes are integral theories for which the general forms for radial distributions of velocity and density defect (and the momentum flux by implication) are presumed to be known in advance. The presumed general forms are chosen to agree with experimental findings. Gaussian forms are most commonly used with the mean velocity and mean density defect given by:

$$u(r,z) = U(z)e^{-r^2/b^2} \tag{1.1}$$

$$\rho_w - \rho_p(r,z) = S(z)e^{-r^2/(\lambda^2 b^2)}. \tag{1.2}$$

where: u is the vertical velocity of the liquid,

z is the height measured upward from the gas outlet,

r is the radius,

U is the centerline velocity,

b is the "plume radius",

ρ_w is the mass density of water,

ρ_p is the mean mass density of the plume,

S is the density effect at the plume centerline,

λ is the ratio of "gas-containing radius" to "plume radius".

Ditmars and Cederwall (1974) developed an integral theory for bubble plumes along the same lines as the integral theory for single phase plumes presented by Morton, Taylor and Turner (1956). Both theories are based on an entrainment hypothesis under which the volume of surrounding liquid that is entrained into the plume per unit height is proportional to both the local centerline velocity and the plume circumference $2\pi b$, with a constant of proportionality being the entrainment coefficient, α. Both theories approximate the plume density as that of the surrounding fluid when calculating the momentum flux and the water mass flux so they contain errors that increase with increasing gas fraction. Also, both theories presume the momentum flux is that of the mean flow so the momentum flux carried by the turbulence is neglected. Differences in the theories are that Ditmars and Cederwall allowed the gas to move more quickly than the liquid by means of a pre-specified "slip velocity" and they included the parameter λ whereas it is absent in the single-phase plume theory of Morton, et. al.

Ditmars and Cederwall made some conclusions about the values of α and λ by comparing their theory to the data of Kobus (1968). However, these must be discounted, particularly those about λ, due to the aforementioned artifacts involved with the Kobus data.

Fannelop and Sjoen (1980) determined both approximate similarity solutions and numerically integrated solutions to a set of equations that neglected the slip velocity of the gas, but otherwise were substantially the same as those used by Ditmars and Cederwall. Fannelop and Sjoen applied their theory to the conditions of their experiments to obtain a comparison between theory and experiment, and to make estimates of the entrainment coefficient, α. This was done by choosing a value of α that was a constant, independent of depth, for each airflow rate such that the error between theory and experiment for plume radius, b, vs height was minimized. They used a value of 0.6 for the gas/velocity radius ratio, λ; where this was based on qualitative photographic observations of the radius of the gas-containing region. The values of α obtained in this way increased with increased gas flow rate; being 0.075 for a gas flow rate of 0.0050 N m^3/s and increasing to 0.102 for a gas flow rate of 0.022 N m^3/s. The comparison between theory and experiment for centerline velocity showed that the theoretical values averaged 15% greater than the experimental measurements.

Milgram and Van Houten (1982) developed a theory that included the effect of gas fraction on mass and momentum fluxes and approximated the turbulent transport of mean momentum flux by assuming that a fixed fraction of this flux was carried by the turbulence. George and Tamanini (1977) found that 8% of the mean momentum flux was carried by the turbulence in their single phase thermal plumes in air. A comparison of velocity measurements and momentum flux measurements in the bubble plumes of Milgram and Van Houten showed that an average of 50% of the mean momentum flux was carried by the turbulence and this value was used in applications of their theory. Bubble "slip velocity" was included in the theory and for the same reasons as are subsequently described here, a value of 0.35 m/s was used for applications. A comparison of measured radial profiles of velocity and gas fraction gave an average value of λ of 0.8 and this value was used in application of the theory. A fixed entrainment coefficient, α was chosen for each gas flow rate in the same way as done by Fannelop and Sjoen. Milgram and Van Houten also found that α increased with increased gas flow rate; being 0.047 for a gas flow rate of 0.000205 N m^3/s and increasing to 0.083 for a gas flow rate of 0.00234 N m^3/s. However, a curve of their values of α vs gas flow rate does not continue smoothly onto a curve for the Fannelop and Sjoen data

which supports the result of dimensional reasoning that other factors besides the gas flow must be involved in determining the entrainment coefficient. The comparison between theory and experiment for the centerline velocity U, vs height for the Milgram and Van Houten study gives agreement without a systematic bias and a normalized standard deviation of about 7%. This completes the review of previous work.

In order to be able to use an integral plume theory to predict the mean velocity and density distributions in a bubble plume of arbitrary depth and gas flow rate, values for four parameters are required. These are the bubble "slip speed" u_b, the gas/velocity radius ratio λ, the entrainment coefficient α, and the ratio of total momentum flux to the momentum flux carried by the mean flow which is called γ. The effects of expected variations from the values of u_b and λ that will be estimated subsequently have been found to be small by numerical tests. A major purpose of this paper is to use experimental results to establish functional relationships between plume properties and α and γ.

2. THEORY

2.1 The Integral Plume Equations

The integral plume theory is based on a principle of local similarity for which radial profiles of velocity have similar forms at different heights as do the radial profiles of density defect. These quantities can then be specified by their centerline values U(z) and S(z); and their characteristic radii, b(z) and $\lambda b(z)$.

The gas is presumed to follow the isothermal expansion law and mean pressure variations on horizontal planes are presumed to be small enough to have only negligible effects on the plume dynamics. Under these conditions, for a liquid of depth H, the gas density, $\rho_g(z)$, is given by

$$\rho_g(z)=\rho_T(H_B-z)/H_T \tag{2.1}$$

where ρ_T is the gas density at a pressure of one atmosphere, H_T is the atmospheric pressure head and H_B is the pressure head at the level of gas release.

$$H_B=H_T+H \tag{2.2}$$

The integral plume equations will involve the local mean gas fraction, f(r,z), which is given by,

$$f(r,z)=\frac{\rho_w-\rho_p(r,z)}{\rho_w-\rho_g(z)} \tag{2.3}$$

and the local gas velocity which will be approximated as the sum of the local liquid speed, u(r,z) and a constant slip velocity, u_b, to approximate the effect of the rise velocity of the bubbles relative to the liquid. q(z), Q(z), M(z) and B(z); the gas volume flux, the liquid volume flux, the momentum flux and the buoyancy per unit height respectively are expressed in terms of local properties as:

$$q(z)=2\pi\int_0^\infty [u(r,z)+u_b]\, f(r,z)\,r\,dr \tag{2.4}$$

$$Q(z)=2\pi\int_0^\infty u(r,z)\,[1-f(r,z)]\,r\,dr \tag{2.5}$$

$$M(z)=2\pi\gamma\int_0^\infty \{u^2(r,z)\rho_w[1-f(r,z)]+[u(r,z)+u_b]^2\,\rho_g(z)f(r,z)\}r\,dr \tag{2.6}$$

$$B(z)=2\pi g\int_0^\infty [\rho_w-\rho_g(z)]f(r,z)\,r\,dr \tag{2.7}$$

γ is called the momentum amplification factor and $(\gamma-1)/\gamma$ is the fraction of the mean momentum flux that is carried in the turbulence. g is the acceleration of gravity.

Closure of the integral plume equations requires a relationship between local plume properties and the rate of increase with height of the liquid volume flux. Ditmars and Cederwall (1974), Fannelop and Sjoen (1980), and Milgram and Van Houten (1982) all used an entrainment hypothesis for the needed relationship and this will be adopted here. It is

$$\frac{dQ}{dz} = 2\pi\alpha b(z)U(z) \tag{2.8}$$

where α is the entrainment coefficient. However, whereas all previous investigators considered the entrainment coefficient as a constant to be specified for any particular plume, here it will be considered to be dependent upon local plume properties.

The three integral plume equations can now be determined. The first is the conservation of liquid equation (2.8). The second is the conservation of gas equation which can be expressed as

$$q_T H_T/(H_B-z) = q(z) \tag{2.9}$$

where q_T is the gas volume flow rate at a pressure of one atmosphere. The third equation results from equating the buoyancy per unit height to the spatial rate of change of momentum flux.

$$B(z) = \frac{dM}{dz} \tag{2.10}$$

2.2 Equations for Gaussian Profiles of Velocity and Density Defect

Experimental evidence shows that the radial profiles of velocity and density defect are well approximated by gaussian curves so equations (1.1) and (1.2) will be used henceforth. For these profiles equations (2.4) through (2.7) become:

$$q(z) = \frac{S(z)\pi\lambda^2 b^2(z)}{\rho_w-\rho_g(z)}\left[\frac{U(z)}{1+\lambda^2} + u_b\right] \tag{2.11}$$

$$Q(z) = \pi U(z)b^2(z)\left\{1 - \frac{\lambda^2 S(z)}{[1+\lambda^2][\rho_w-\rho_g(z)]}\right\} \tag{2.12}$$

$$M(z)=\pi b^2(z)\gamma\left\{U^2(z)\left[\frac{\rho_w}{2}-\frac{\lambda^2 S(z)}{1+2\lambda^2}\right]+\frac{\lambda^2 u_b \rho_g(z) S(z)}{\rho_w-\rho_g(z)}\left[\frac{2U(z)}{1+\lambda^2}+u_b\right]\right\} \quad (2.13)$$

$$B(z)=\pi g\lambda^2 S(z) b^2(z) \quad (2.14)$$

The plume equations (2.8), (2.9) and (2.10) then become:

$$2\alpha U(z)b(z) = \frac{d}{dz}U(z)b^2(z)\left\{1-\frac{\lambda^2 S(z)}{[1+\lambda^2][\rho_w+\rho_g(z)]}\right\} \quad (2.15)$$

$$\frac{q_T H_T}{H_B-z} = \frac{\pi\lambda^2 b^2(z) S(z)}{\rho_w-\rho_g(z)}\left[\frac{U(z)}{1+\lambda^2}+u_b\right] \quad (2.16)$$

$$g\lambda^2 S(z)b^2(z) = \frac{d}{dz}\gamma b^2(z)\left\{U^2(z)\left[\frac{\rho_w}{2}-\frac{\lambda^2 S(z)}{1+2\lambda^2}\right]+\frac{\lambda^2 u_b \rho_g(z) S(z)}{\rho_w-\rho_g(z)}\left[\frac{2U(z)}{1+\lambda^2}+u_b\right]\right\} \quad (2.17)$$

with $\rho_g(z)$ given by equation (2.1).

2.3 Initial Conditions Near the Bottom of the Zone of Established Flow

Equations (2.15), (2.16) and (2.17) can be integrated upward numerically if all parameters are known and if conditions near the bottom of the zone of established flow are known so that the integration can be started. Equation (2.16) for the conservation of gas is valid so two additional conditions are required. The precise determination of these requires unavailable information about the zone of flow establishment, but suitable approximations for most conditions can be made. The reasons for this are that over most of the extent of the plume the momentum gained in the zone of established flow dominates the momentum gained in the zone of flow establishment, and solutions to the plume equations are generally particularly stable to perturbations in initial conditions.

The momentum flux at the height where the integration is to be started, z_E, is estimated as the sum of the momentum flux coming from the gas outlet and an estimate of the buoyancy in the zone beneath this height. To minimize the error of this estimate, z_E should be chosen as low as possible so that the buoyancy beneath it is minimized. However, as the height of the gas outlet is approached there is expected to be more error in the first part of the integration due to inaccuracies in both the gaussian approximations and the entrainment hypothesis.

The best choice for z_E is the one which gives the best balance between these influences. Although this is not known exactly a reasonable position would seem to be the greater of five gas outlet diameters, D, and the height of the zone of flow establishment for single phase plumes given by Chen and Rodi (1980). This is:

$$z_E = \min \left(\begin{matrix} 5D \\ 10u_o(D/g)^{\frac{1}{2}}[\rho_g(o)/\rho_w]^{\frac{3}{4}} \end{matrix} \right) \qquad (2.18)$$

where u_o is the gas velocity at the outlet as determined from the gas volume flow rate and the area of the gas outlet.

Estimating the mean gas speed below $z = z_E$ as $u_o/2$, the estimate for the momentum flux becomes:

$$M(z_E) = q_T \rho_g(H) u_o + \frac{2q(z_E/2)}{u_o} [\rho_w - \rho_g(z_E/2)] g z_e \qquad (2.19)$$

Finally, the centerline plume density defect is estimated as:

$$S(z_E) = \rho_w/2 \qquad (2.20)$$

It must be emphasized that these cavalier estimates of $M(z_E)$ and $S(z_E)$ are not represented as accurate values for the top of the zone of flow establishment, but rather are reasonable values for beginning the numerical integration at $z = z_E$. Figure 2.1 is an example of the insensitivity of results over most of the plume of the numerical integration to reasonable variations in the initial conditions.

2.4 Theoretical Framework for Analysis of Velocity Measurements

The measurement data which will be used to determine the relationship between local plume properties and both the entrainment coefficient, α, and momentum flux amplification factor, γ, are the laboratory experiments of Fannelop and Sjoen (1980) and of Milgram and Van Houten (1982) as well as the larger scale experiments described subsequently. All of these experiments included measurements of radial profiles of vertical velocity, but profiles of gas fraction and momentum flux were only measured in the second study. For the other experiments these quantities must be determined by application of the plume theory to the velocity measurements, and for consistency this procedure will be applied to all of the data. Application of the theory requires a priori specification of the bubble "slip velocity" u_b, and of the gas/velocity radius ratio, λ.

Photographic measurements of bubble sizes made by the author (for air bubble plumes in water) showed that most of the gas was carried by bubbles whose volumes ranged from 0.01 to 33 cm^3. Of these, most of the bubbles had volumes between 0.02 and 0.5 cm^3 for which Haberman and Morton (1954) found rise velocities in still water between 0.23 and 0.25 m/s. However, the larger and faster moving bubbles contain much more volume than the smaller bubbles and Haberman and Morton found a rise velocity of 0.45 m/s for 33 cm^3 bubbles. For the subsequent application of the theory here, a value of 0.35 m/s is used. Figure 2.2 shows an example of the results of numerical integration of the plume equations (2.15), (2.16) and (2.17) for four different values of u_b; 0.00, 0.30, 0.35 and 0.40 m/s. The effect of ± 0.05 m/s variation in u_b is small, but clearly u_b cannot be discounted altogether.

By comparing measured gas fraction profiles with measured velocity profiles, Milgram and Van Houten found an average value for λ of 0.8 for their laboratory experiments. No other experimental values are available. However, under the presumption that turbulent velocities scale with mean velocities, λ is expected to be larger (but still less than 1.0) for the other plumes to be considered here since they are larger and faster than the Milgram and Van Houten plumes. Figure 2.3 shows an example with values of both 0.8 and 0.9 for γ. The effect of the variation is quite small and a value of 0.8 will be used here in the analysis of the measurements.

The gaussian approximations given by equations (1.1) and (1.2) for radial profiles of velocity and density defect will be used. For each measured radial profile at a height z, U(z) and b(z) are determined by a fit of equation (1.1) to the data. The local gas density is given by equation (2.1) and the local gas volume flow rate is given by the left hand side of equation (2.16). The local density defect can then be determined from equation (2.11) as,

$$S(z) = \frac{[\rho_w - \rho_g(z)]q(z)}{\pi\lambda^2 b^2(z)[U(z)/(1+\lambda^2) + u_b]} \qquad (2.21)$$

The local momentum amplification factor, $\gamma(z)$ will be obtained as the ratio of the total local momentum flux, M_T, to the momentum flux of the mean flow, M_m.

$$\gamma(z) = \frac{M_T(z)}{M_m(z)} \qquad (2.22)$$

where $M_m(z)$ is obtained from equation (2.13) with γ set equal to 1.

The total momentum flux at height z will be calculated as,

$$M_T(z) = M_T(z_B) + \int_{z_B}^{z} B(z')dz' \qquad (2.23)$$

where the buoyancy per unit height, B(z), is given by equation (2.14).

The height z_B will be taken as the lowest height in the zone of established flow at which conditions are measured or estimated. The momentum flux at z_B is estimated in the fashion of equation (2.19), but since z_B is generally considerably greater than z_E a different estimate for the mean gas speed below z_B is required. Within a short distance above the height of gas release, the moving material involves a volume flux of water that is of the same order of magnitude as the volume flux of the gas. Therefore the average gas speed below z_B will be estimated as the average of $u_o\rho_g(z_B/2)/\rho_w$ and $[U(z_B) + u_b]$. Then,

$$M_T(z_B)=q_T\rho_T u_o + 2q(z_B/2)gz_B[\rho_w-\rho_g(z_B/2)]/[u_o\rho_g(z_B/2)/\rho_w+U(z_B) + u_b] \qquad (2.24)$$

Because of uncertainty of the buoyancy below z_B, M_T evaluated in this way cannot be expected to be accurate enough for quantitative estimates of γ at z_B. For all measurement heights above z_B that are used, $M_T(z)>>M_T(z_B)$ so that equation (2.23) is expected to be accurate enough for making quantitative estimates of γ by use of equation (2.22).

The other parameter which depends on local conditions to be determined from the experiments is the entrainment coefficient, α. Although it could be obtained from experimental determination of the terms in equation (2.8), the differentiation of the liquid volume flux would accentuate experimental errors. To avoid this, α will be determined by an integration of equation (2.8) between heights at which radial velocity profiles are measured. Call these heights z_i (i=1,2,...). Then, under the presumptions that α varies only slightly between z_i and z_{i+1} and that the liquid volume flux, Q, is well approximated by a linear function in this same height interval, the integral of equation (2.8) is solved for α as

$$\alpha\left(\frac{z_i+z_{i+1}}{2}\right) = \frac{2}{\pi}\frac{Q(z_{i+1}) - Q(z_i)}{[b(z_i)+b(z_{i+1})][U(z_i)+U(z_{i+1})][z_{i+1}-z_i]} \qquad (2.25)$$

where Q(z) is given by equation (2.12).

3. EXPERIMENTS

3.1 Facility and Equipment

In order to increase the range of scales of bubble plume data, experiments for measuring velocity profiles were conducted with a gas outlet depth of 50 meters and gas flow rates up to 0.59 N m^3/s. The experiments took place in Bugg Spring which is a natural sinkhole spring located at Okahumpka, Florida and which is part of the United States Naval Research Laboratory. Figure 3.1 is a cross-sectional profile of the spring. Both currents and spatial temperature variations in the spring are smaller than can be measured with ordinary instruments. A barge which is tightly moored to anchors on the shore by five cables floats on the surface with one edge of the barge over the deepest part of the spring. An existing gantry was extended to a distance of 4.6 m past this edge. A 2.5 meter tall vertical air entry pipe having a 5 cm inside diameter was secured to a concrete anchor block such that the upper open end of the pipe was 50 m below the surface and vertically under the extended end of the gantry. Air was supplied to the bottom of the pipe through a hose from an airflow meter on the barge which in turn was connected by a hose to a rotary screw air compressor on the shore.

Velocity profiles were measured with the use of a horizontal array of 36 vertical current meters configured as a cross as shown in figure 3.2. Each of the two arms of the cross was 12.9 meters long and the distance between adjacent current meters was 0.75m. This permitted an accurate estimation of the location of the instantaneous center of the plume from the location on each of the arms on the cross at which the velocity was a maximum.

A system of four support cables was used to adjust the height of the cross and to provide horizontal restraint against turbulence-induced motions of the cross. A taut upper cable attached the upper bridle shown in figure 3.2 to the gantry. A taught lower cable attached to the lower bridle passed through a sheave near the air outlet and then to the barge. Two adjacent ends of the cross rode on vertical cables tensioned to about 10^4 newtons which led from the edge of the barge to anchor weights on the bottom.

The current meters were made from the mechanical speed detecting parts of Aanderaa current meters and 36 electronic signal conditioners, each of which contained a low-pass filter with a 10 second time constant. The resulting signals were sampled at a rate of 1 Hz through 36 analog-to-digital channels of a digital computer for 10 minutes for each airflow rate and current meter cross height. Each of the groups of 36 samples was obtained in a time interval of about 0.5 millisecond

so the samples can be considered to be simultaneous. Finally, for each channel each set of ten successive samples was averaged together giving 60 of these short-time averaged measurements for each of the 36 channels in a ten minute measurement period. These measurements were made for airflow rates of 0.024, 0.118, 0.283 and 0.590 N m^3/s; and for heights above the air outlet of 16.47, 25.62, 37.81, 43.90 and 46.95 meters.

3.2 Data Reduction

The purpose of the data reduction was to fit a gaussian function as given in equation (1.1) to every radial profile measured with respect to the instantaneous location of the plume centerline and thereby obtain values for the centerline velocity, U, and the plume radius, b. This was done by the following steps:

1. For each 36 point, 10 second velocity average, there were 18 values along one axis of the measuring cross and 18 values along the other. Spline cubic interpolating functions were fit to each of these 18 sets of points. The location of the maximum of each of these functions was taken as the value in "cross coordinates" for the location of the plume center. The distance from this location to each of the current meters was determined so that 36 sets of values (u,r) were obtained. This was done for all 60 sets of 10 second averages so that 2160 pairs of (u,r) values were obtained for each airflow rate and measurement height.
2. The range of values of radius, r, was partitioned into segments 0.08 meters long. The values of u for all the r values falling in any particular segment were averaged together to obtain a value of u for the midpoint of the segment. This reduced the number of pairs of (u,r) values for each airflow rate and measurement height to about 100. Figure 3.3 shows an example of a plot of these values.
3. A gaussian function of the form of equation (1.1) was fit to the reduced data points with U and b chosen to minimize the standard deviation between the function and the points. Figure 3.3 shows the gaussian approximation to its data.
4. The above procedure gave 20 radial profiles of velocity. The one for a measurement height of 46.95 m at an airflow rate of 0.118 N m^3/s was "out of line" with other profiles and the measured profile had excessive scatter. Therefore this profile was eliminated from the data leaving 19 of these larger scale profiles available for analysis.

5. The current meters measured velocities in the (r,z) plane. Since the radial mean velocities are small in comparison to the vertical mean velocities, their effects on the measured mean velocities are small. However, a small correction can be, and was, made for this. For each airflow rate the values of $b(z)$ and $U(z)$ were fit by spline cubic functions so that their derivatives could be easily evaluated. Then, using the form of equation (1.1) and a radial integration of the continuity equation (div $\vec{V}=0$, neglecting here the effects of the variation in mean density) gave the small radial velocity. From this and the measured velocities in the (r,z) plane, the vertical velocity components were calculated. These radial profiles of vertical velocity were then fit with gaussian curves as before. The results are shown in table 1.

4. DATA ANALYSIS

4.1 The Data Set

The goals of the data analysis are the determinations of functional relationships between local plume properties and the entrainment coefficient, α, and the momentum amplification factor, γ. The experimental measurements used for this are the relatively small scale measurements of Milgram and Van Houten (1982), the measurements at about three times larger scale of Fannelop and Sjoen (1980) and the measurements at about fifteen times larger scale made in Bugg Spring. Each of these sets of measurements contains several radial profiles of vertical velocity at each of several airflow rates with these profiles approximated by gaussian functions of the form of equation (1.1). Thus the data to be used here are in the form of values $b(z)$ and $U(z)$ at each airflow rate.

For the Fannelop and Sjoen experiments the lowest measurement height was 6.5% of the gas outlet depth, whereas for the Milgram and Van Houten experiments and for the Bugg Spring experiments the equivalent percentages were 26% and 32% respectively. The percentage is small enough for equation (2.24) to be applied at the lowest height for the Fannelop and Sjoen experiments, but this is not the case for the two latter experiments. In these cases, conditions at adequately low points were estimated by an application of the integral theory. This was done as follows. For each airflow rate, the plume equations (2.15), (2.16) and (2.17) were numerically integrated several times starting at a height z_E as given by equation (2.18); each time with different values of α and γ which were taken, for this step only, to be independent of height. The integration which best fit the measured values of $b(z)$ and $U(z)$ was chosen in each case. An example of this is shown in figure 4.1. As is demonstrated in figure 2.1, errors in initial conditions for beginning the integration are most influential in the region below the minimum (maximum negative) slope of the function $U(z)$. Therefore, a value of z_B was chosen for application of equation (2.24) that was above this point of minimum slope and the required values of $U(z_B)$ and $b(z_B)$ were obtained from the numerical integration. The values used for z_B were 0.32 meters for the Milgram and Van Houten experiments and 1.98 m for the Bugg Spring experiments.

For all three sets of experiments, values of $b(z)$ and $U(z)$ were fit with spline cubic functions. Instead of forcing these functions to fit all the data points exactly, functions with four equally spaced nodal points with extrapolated end point curvatures were used subject to the criterion of minimum variance with the unsmoothed data. Since data at five or six heights were used, this process introduced a small amount of data smoothing. The spline cubic

functions were used for the remainder of the data analysis. Table 1 shows both the unsmoothed data and the evaluations of the spline cubic functions. At each data height these evaluations were used together with equations (2.21) and (2.14) to determine the centerline density defect and the buoyancy per unit height which was then in turn fit with a four nodal point cubic spline function. This was then integrated by quadrature to evaluate equation (2.23) at each data height. With this done, the momentum amplification factor was evaluated from equation (2.22) at each data height except for the z_B's and these values are also shown in table 4.1. Finally, table 1 shows the values of the liquid volume flux, Q(z) which were determined from equation (2.12).

The values of the entrainment coefficient, α, were determined from equation (2.25) at positions midway between data heights and these are shown in table 2. Values of both α and γ for the highest measurement point at the two largest gas flow rates in the Milgram and Van Houten data appear "out of line" with other values. Therefore these two data rows for both the α and γ data are not used in the subsequent data analysis. They are shown in tables 4.1 and 4.2 because they were used in the raw data set.

4.2 The Entrainment Coefficient

For single phase plumes many investigators have proposed a constant value for the entrainment coefficient, while others (c.f. Fox, 1974; or Seban and Behnia, 1976) have suggested a functional relationship between local plume properties and the entrainment coefficient of the form,

$$\alpha_{\substack{\text{single}\\\text{phase}}} = K_1 + K_2/(F_r)^2 \tag{4.1}$$

where K_1 and K_2 are constants and the densiometric plume radius Froude Number is given in terms of the variables used here as,

$$F_r = U\sqrt{\rho_w/gbS} \tag{4.2}$$

The entrainment coefficients for bubble plumes in the data set are not constants and a quantitative comparison with equation (4.1) shows that this functional relationship does not apply to bubble plumes. Therefore, the approach taken here is to determine an empirical functional relationship between dimensionless local plume properties and the entrainment coefficient, based on the measured data and a few simple concepts.

It is assumed that the viscous forces are small in comparison to pressure, inertia and surface tension forces. Then the local independent variables are b, g, S, $\rho_w-\rho_g$, u_b, T and (U or q). Either U or q can be taken as independent, but not both. The relationship between the entrainment coefficient and each dimensionless grouping of these variables with rational exponents whose denominators were 10 or less was examined and the one giving the best collapse of the data is $\Delta^{1/3} q^{2/5} g^{3/10} (\rho_w-\rho_g)^{1/2} T^{-1/2}$

where Δ is the centerline gas fraction

$$\Delta = S/(\rho_w-\rho_g) \quad . \tag{4.3}$$

This dimensionless group will be called the bubble Froude number, F_B, and it can be expressed as:

$$F_B = L_m/L_D \quad . \tag{4.4}$$

where

$$L_m = (q^2/g)^{1/5} \tag{4.5}$$

and

$$L_D = \frac{\sqrt{T/g(\rho_w-\rho_g)}}{\Delta^{1/3}} \tag{4.6}$$

L_m is the mixing distance of bubble motions in the turbulence inasmuch as it is the scale of the distance that gas bubbles moving at the characteristic speed $(g^2q)^{1/5}$ can penetrate downward against the gravitational hydrostatic pressure. L_D is the characteristic distance between bubbles since $\sqrt{T/g(\rho_w-\rho_g)}$ is the characteristic length scale of a bubble.

Figure 4.2 shows the data points of α vs F_B. In addition to the data points, two additional conditions were used in determining a form for a functional relationship between α and F_B. These are

1. As $F_B \to 0$ the plume becomes an occasional single bubble with no difference in wake conditions between one height and another. For this limit the entrainment coefficient must be zero.
2. As $F_B \to \infty$ the bubbles are close to each other and the plume must act as a single phase plume. For this limit the entrainment coefficient relationship will be required to approach equation (4.1). A functional relationship which

meets these conditions and which is consistent with the trend of the data in figure 4.2 is

$$\alpha(F_B,F_r)= \{(F_B)^{A_1}/[A_2+F_B)^{A_1}]\}\{K_1+K_2/(F_r)^2\} \qquad (4.7)$$

For fitting equation (4.7) to the data in table 4.2 each data point α_j was assigned a weight W_j taken as the ratio of the vertical distance $z_{i+1}-z_i$ used in equation (2.25) for evaluating α_j to the total depth H. The constants A_1, A_2, K_1 and K_2 were chosen so as to minimize the weighted square error E_α^2 over the 53 data points of table 2 which were used.

$$E_\alpha^2 = \sum_{j=1}^{53} W_j[\alpha_j - \alpha(F_B,F_r)]^2 \qquad (4.8)$$

The value of K_2 found by this process was so small that, over the range of data points, the K_2-term in equation (4.7) varied from 2% to 6% of the K_1-term. The value found for A_1 was 0.95. Because of these findings and the fact that the data is neither comprehensive enough or accurate enough to predict α in complete detail, it was deemed appropriate to set K_2 to zero and A_1 to 1 and thereby replace equation (4.7) with the simpler form:

$$\alpha(F_B) = K\frac{F_B}{A+F_B} \qquad (4.9)$$

The weighted error minimization process was then repeated with the results,

$$K = 0.165 \qquad A = 7.598 \qquad (4.10\ a,b)$$

Figure 4.2 shows the function $\alpha(F_B)$.

Much of the scatter of the data points in figure 4.2 has been found to result from small variations from smooth functions in the measured values of b vs z. This scatter can be greatly reduced by a consideration of averages over height. For each experiment at a fixed airflow rate, the bubble Froude numbers at different heights vary by up to 25% from their height-average as a rule. This variation is small enough to allow a comparison of height-averaged entrainment coefficient with height-averaged bubble Froude number to be useful. In forming these height averages, the individual quantities were weighted in accordance with the values of W given in Table 2. Figure 4.3 shows the height-averaged data points. A function of the form of equation (4.9) was fit to these

data and the best (minimum RMS error) fit was obtained with K = 0.165 and A = 7.907. Figure 4.3 shows both this function as well as the previous fit to the individual data points with A = 7.598. The fact that the difference is so small means that the influence of the scatter on the functional fit can be neglected and the values given in equation (4.10) will be used in subsequent sample calculations.

4.3 The Momentum Amplification Factor

A similar process was used to find an empirical function for the momentum amplification factor, γ. The dimensionless grouping of the independent variables giving the best collapse of the data of table 4.1 is $U^2(\rho_w-\rho_g)^{1/2} g^{-1/2} \Delta^{-2/3} T^{-1/2}$. This quantity will be called the phase distribution number, N_P, and it can be expressed as

$$N_P = L_V/L_D \tag{4.11}$$

where L_V is the vertical length scale of the plume motion,

$$L_V = U^2/g\Delta \tag{4.12}$$

Figure 4.4 shows the data points of γ vs N_P. For determining the form of a functional relationship between γ and N_P two conditions were used in addition to the data points. These are:

1. As $N_P \to 0$ the plume degenerates to an occasional single bubble. In this limit, γ, the ratio of total momentum flux to the momentum flux in the mean flow becomes large without limit.
2. As $N_P \to \infty$ the bubbles are very closely spaced and the plume must act like a single phase plume. Most single phase plume investigations have been based on $\gamma=1$ although the measurements of George and Taminini (1977), indicate $\gamma = 1.07$. Data fits for both asymptotic limits were determined.

Functional relationships which meet the above conditions and are consistent with the trend of the data points in figure 4.4 are:

$$\gamma(N_P) = 1.0 + C_1/(N_P)^{C_2} \tag{4.13}$$

and

$$\gamma(N_P) = 1.07 + D_1/(N_P)^{D_2} \tag{4.14}$$

Experimental values of γ were not evaluated at the lowest of each set of data heights shown in table 4.1 because of the large influence at these heights of potential errors in the estimate of the buoyancy beneath them. Also the two aforementioned "out of line" points in the Milgram and Van Houten data were excluded. This leaves 53 data points. C_1, C_2, D_1 and D_2 were determined so as to minimize E_γ^2, which is the square error over these 53 points.

$$E_\gamma^2 = \sum_{j=1}^{53} [\gamma_j - \gamma(N_P)]^2 \qquad (4.15)$$

No weighting function of height differences was used in this case because the experimental evaluations of γ do not depend directly on measured differences at two adjacent measurement heights as was the case with α.

The values obtained for C_1, C_2, D_1 and D_2 are:

$$C_1 = 337.7 \qquad C_2 = 1.25 \qquad (4.15\ a,b)$$

$$D_1 = 977 \qquad D_2 = 1.5$$

Figure 4.4 shows these functional relationships.

4.4 Results from Other Experiments

The subsonic orifice data of Kobus (1968) and the data of Topham (1975) were analyzed in precisely the same way as done with the primary data set. Tables 3 and 4 for the Kobus and Topham data are analagous to tables 1 and 2 for the primary data set. The calculated values of α and γ for the Kobus data are also shown in figures 4.2, 4.3 and 4.4. The γ values for the Topham data are not reasonable. The α values for the Topham data have unreasonable variations with height due to the irregular shapes of b vs z. However, the height-averaged values of α for the Topham data are reasonable and these are shown on figures 4.2 and 4.3.

5. PLUME WANDERING

If a radial profile of a physical quantity in a bubble plume is measured by a set of long-term time averages, each at a radius reckoned with respect to a vertical line above the gas outlet, plume wandering can influence the measurements. In the presence of plume wandering, such a measured profile will generally have a smaller centerline value and a larger width than a profile reckoned with respect to the instantaneous location of the centerline.

5.1 Mathematical Model

Consider a horizontal plane (X,Y) through a bubble plume whose vertical velocity profile is given by:

$$u = Ue^{-\frac{x^2+y^2}{b^2}} \tag{5.1}$$

where x and y are horizontal coordinates relative to the instantaneous centerline location. Furthermore, suppose the location of the centerline is a joint gaussian random variable (ξ,η) whose probability density function is given by:

$$p_{\xi\eta}(\xi_o,\eta_o) = \frac{1}{\pi\sigma^2} e^{-\frac{\xi_o^2+\eta_o^2}{\sigma^2}} \tag{5.2}$$

where

$$\sigma^2 = \overline{\xi^2+\eta^2} \tag{5.3}$$

the overbar designating the statistical average.

Let the origin of the (X,Y) plane be at the mean centerline location and consider measurements along Y=0 which will be called u_L.

$$u_L(X) = Ue^{-\frac{(X-\xi_o)^2+\eta_o^2}{b^2}} \tag{5.4}$$

The statistical average of u_L, which is representative of the long-term time average of u_L is:

$$\overline{u_L(X)} = \int_{-\infty}^{\infty}\int_{-\infty}^{\infty} u_L p_{\xi\eta}(\xi_o,\eta_o)d\xi_o d\eta_o \tag{5.5}$$

Carrying out the integration results in:

$$\overline{u_L(X)} = U_L e^{-\frac{X^2}{b_L^2}} \tag{5.6}$$

where $$U_L = U/(1 + \frac{\sigma^2}{b^2}) \tag{5.7}$$

and $$b_L = b\sqrt{1+\sigma^2/b^2} \tag{5.8}$$

Since the plume width, b, at any height is a monotonically increasing function of values of the entrainment coefficient, α, below this height; plume wandering will result in overestimates of α if they are based on long-term time averages.

Let γ_L be the momentum flux amplification factor based on the long-term time average measurements, U_L and b_L. Then, for the usual case of ($f<<1$, $\rho_g<<\rho_w$), application of equation (2.22) gives:

$$\gamma_L = \gamma(1 + \frac{\sigma^2}{b^2})^{\varepsilon} \tag{5.9}$$

where $1 \leq \varepsilon \leq 2$ and ε increases with increasing $U/[u_b(1+\lambda^2)]$. Therefore, if a plume wanders, the momentum flux amplification factor is expected to be overestimated if it is based on measurements of long-term time averages.

5.2 Considerations of the Experiments

Fazal (1980) measured long-term time averages of momentum flux and gas fraction at an airflow rate of 0.0023 N m^3/s in the same tank as was later used by Milgram and Van Houten (1982). The momentum flux sensor used was subsequently found to undergo random zero shifts so its data will not be considered here. The calibration of the gas fraction sensor used is uncertain so the magnitude of the gas fraction will not be considered. However, the gas fraction profile radii, the λb's, can be compared to those later found with respect to the instantaneous centerline location to show the influence of plume wandering. These radii were determined for use here by fitting a gaussian curve to each of the gas fraction profiles. The lowest height at which Milgram and Van Houten measured gas fractions at an airflow rate of 0.023 N m^3/s was 1.58 m. To obtain estimates lower in the plume the value of b from the velocity data at a height of 0.96 m was multiplied by 0.8 (the estimate of λ), and the calculated result at 0.32 m (z_B) was included. Figure 5.1 shows the results for both the long-term time averaged data and the data with respect to the instantaneous centerline location. The radii from the long-term time averages are clearly wider which supports the visual observations of plume wandering in the tank and the need to measure the plume properties with respect to the

instantaneous centerline location. This was done for both the Milgram and Van Houten experiments and for the larger scale Bugg Spring experiments.

The data of Fannelop and Sjoen, which were in the form of long-term time averages were included here in the primary data set used to determine the relationship between plume properties and α and γ. This is only justifiable if those data were not materially influenced by plume wandering. A test of this influence was provided by determining the relationship between plume properties and α and γ with the Fannelop and Sjoen data removed from the data set. There was essentially no change in the best relationship between plume properties and α. Equation (4.9) still provided the best relationship with $K = 0.165$. The only change was that the constant A changed from the value of 7.598 to 7.515. The best relationship between plume properties and γ was provided by equation (4.13) with $C_1 = 111.3$ and $C_2 = 1.0$. A graph of this function is shown in figure 4.3. The relationships between plume properties and α and γ are so little changed by exclusion of the Fannelop and Sjoen data that it is likely these data were not materially influenced by plume wandering.

The evidence concerning the influence of plume wandering on the data of Kobus (1968) is mixed. Although these data were not used in determining functional relationships between plume properties and α and γ, values of α and γ calculated from them are shown in figures 4.2 and 4.3. The values of α shown in figure 4.2 for the Kobus data are definitely larger than the other data and the functional relationship would predict. This indicates a possible influence by plume wandering. However, the values of γ shown in figure 4.3 for the Kobus data are not, for the most part, higher than other data would predict. Since this indicates a lack of influence by wandering the evidence is mixed and no clear conclusions of the influence of wandering on the Kobus data can be drawn.

The analysis of the Bugg Spring data included determination of the location of the plume center for each of the 60 sets of data points used in the determination of each radial profile of vertical velocity. These 60 values of center location were used for experimental determination of σ, the variance of the radial location of the plume center. For each height at each gas flow rate the quantity $(1+\sigma^2/b^2)$ (see equations 5.7 and 5.8) was determined. This quantity ranged from 1.004 to 1.092 with an average value of 1.040. This indicates that only a modest amount of plume wandering occurred in the Bugg Spring experiments although even it was taken into account by reckoning the data with respect to the instantaneous location of the plume centerline.

6. APPLICATION

By combining the semi-empirically determined functional relations between local plume properties and the entrainment coefficient, α, and the momentum amplification factor, γ, with the plume equations (2.15), (2.16) and (2.17); numerical solutions can be obtained without the need for a priori specification of α and γ.

Previous experiments for determining the speed of single air bubbles in water indicate a bubble slip speed of about 0.35 m/s. Since the surface tension of natural gas against water is similar to that of air against water unless the pressure is very large, gas bubble sizes in subsea well blowouts are expected to be similar to air bubble sizes unless the depth is very great. Bishnoi and Maini (1979) determined the downward flow speed of water to keep natural gas bubbles stationary in a vertical tube. These data suggest a bubble slip speed of about 0.26 m/s, but after they are corrected for tube blockage by the bubble the indicated slip speed is about 0.28 m/s. The difference in numerical results between cases with $u_b = 0.35$ and $u_b = 0.28$ is slight and 0.35 m/s will be used for the applications here.

The gas/velocity radius ratio, λ, is expected to increase with increasing values of the ratio of plume velocity to slip velocity U/u_b. For relatively small plumes with $0.9<U/u_b<2.9$ previous measurements show $\lambda \approx 0.8$. The solution to the plume equations changes only slightly when λ changes from 0.8 to 0.9. Since λ is not expected to exceed 1.0 use of $0.8 \leq \lambda \leq 0.9$ is appropriate except for very small and slow plumes ($U/u_b < 0.5$). A value of 0.8 will be used here.

The numerical solution to the plume equations with the formulations described above for the experiment of Milgram and Van Houten (1982) at an airflow rate of 0.00050 N m^3/s is shown in figure 6.1. The measured values of U, b and centerline gas fraction are also shown in the figure. The agreement is quite good, but not as good as occurs when specific values of α and γ are chosen to give the best agreement between theory and experiment.

Figure 6.2 shows the numerical solution for conditions of a subsea well blowout of 10 N m^3/s of gas at a depth of 100 m through an 0.05 m^2 opening. Although there is no quantitative data for the flow above blowouts, the results are in qualitative agreement with what is observed.

7. CONCLUDING DISCUSSION

The integral mean flow plume equations (2.15), (2.16) and (2.17) using gaussian radial profiles are applicable to bubble plumes over a wide range of scales. There are four parameters in the theory. u_b, λ, α and γ. Two of them; the bubble slip speed u_b, and the gas/velocity radius ratio, λ, can be estimated from known information to be approximately 0.35 m/s and 0.8 respectively. Since modest changes in values of u_b or λ result in only a small change in the solution to the plume equations, these estimates can be quite approximate. Nonetheless, it would be of interest to confirm in a large scale experiment the expectation that λ approaches 1.0 for large values of U/u_b whereas it has been found to be approximately 0.8 at small scale.

Semi-empirical functional relationships between local plume properties and the entrainment coefficient, α, and for the momentum amplification factor, γ, have been determined. When these relationships for α and γ and the aforementioned approximations for λ and u_b, are combined with the plume equations (2.15), (2.16) and (2.17), the theory takes a closed form that can be applied to any round bubble plume.

It is of interest to speculate on the possible physical bases for the relationships between plume properties and α and γ. Since there is no conclusive evidence which supports these speculations and eliminates all others, they must be considered as tentative. α is small for small bubble Froude numbers which occurs when the bubbles are widely spaced in comparison to the characteristic mixing distance of the bubbles in the fluid. For this condition, the bubbles must act more or less individually. When the bubbles are closely spaced in comparison to the bubble mixing distance the bubble wakes are merged and the plume is more of a unified moving water plume so the entrainment is similar to that of a single phase plume.

L_V is the characteristic distance the mean flow must move in order for the buoyancy to make a significant change in plume properties. When this distance is large in comparison to the characteristic distance between bubbles, which are the sources of buoyancy, the buoyancy and its resulting momentum flux are well diffused through the plume. This is the case of a large phase distribution factor with nearly all of the momentum flux carried in the mean flow. When L_V is not large in comparison to the characteristic distance between bubbles, the buoyancy sources and their resulting momentum fluxes are more separated and distinct which leads to a higher fraction of the momentum flux carried by the fluctuating variations of velocity.

The smallest scale laboratory experiments which have taken place have had small enough phase distribution factors, N_p for the momentum flux amplification factor to be significantly greater than 1.0. However, the largest scale laboratory experiments have had large enough phase distribution factors for γ to be nearly equal to 1.0. The available data shows that γ is close to 1.0 when N_p exceeds 800 which would nearly always be the case for subsea well blowouts.

Small scale laboratory tests have had considerably smaller entrainment coefficients than are expected for blowouts of gas-containing subsea wells which result in much larger bubble Froude numbers. Available data suggests that the entrainment coefficient is relatively constant for bubble Froude numbers in excess of 50. However, very large scale experiments are needed to confirm this.

Plume wandering was severe enough with a gas outlet depth of 3.66 m in the 1.65 m diameter tank used by Milgram and Van Houten (1982) to necessitate special steps to measure data with respect to the instantaneous location of the moving centerline. With the exception of the mixed evidence concerning the influence of wandering on the data of Kobus (1968), wandering did not significantly influence the results of other experiments. It seems most likely that large amplitude wandering is due to the effects of the tank walls when the horizontal extent of the facility is not very large in comparison to the plume diameter. These effects may be due to direct interaction between the plume and the sidewalls or to interactions involving the return flow in the tank. Because of the mixed evidence concerning the effects of wandering on the Kobus data, complete confirmation that large amplitude wandering requires the influence of close sidewalls requires an experiment on small scale plumes in a tank of large horizontal extent.

ACKNOWLEDGEMENTS

This study was supported, in part by the U.S. Department of the Interior under contract number 14-08-001-20460, and in part by the Office of Naval Research under contract number N00014-81-K-0785.

R E F E R E N C E S

BISHNOI & MAINI 1979 Laboratory study of behavior of oil and gas particles in salt water relating to deep oil well blowouts. Spill Technology Newsletter. Environmental Protection Service, Hull, Quebec, #EPS-3-ED-80-1, 4[1], 24-36.

CHEN, C.J. & RODI, W. 1980 Vertical turbulent buoyant jets, a review of experimental data. HMT - The Science and Application of Heat and Mass Transfer - Reports, Reviews & Computer Programs. Pergamon Press.

DITMARS, J.D. & CEDERWALL, K. 1974 Analysis of air-bubble plumes. Coastal Engineering Conference. Chapter 128, 2209-2226.

FANNELOP, T.K. & SJOEN, K. 1980 Hydrodynamics of underwater blowouts. AIAA 18th Aerospace Sciences Meeting. Pasadena, CA.

FAZAL, R. 1980 Gas bubble plumes in water. MIT Engineer Degree Thesis. Cambridge, Massachusetts

FOX, D.C. 1970 Forced plume in a stratified fluid. J. of Geophysical Research 75 No. 33, 6818-6835.

GEORGE, W.K. & ALPERT, R.L., & TAMANINI, F. 1977 Turbulence measurements in an axisymmetric buoyant plume. J. of Heat Mass Transfer 20, 1145-1154.

HABERMAN, W.L. & MORTON, R.K. 1954 An experimental study of bubbles moving in liquids. Proc. of the Amer. Soc. of Civil Eng. 80, Separate #387.

KOBUS, H.E. 1968 Analysis of the flow induced by air-bubble systems. Coastal Engineering Conference, London. II, Ch. 65, 1016-1031.

MILGRAM, J.H. & VAN HOUTEN, R.J. 1982 Plumes from sub-sea well blowouts. Proc. of the Third Int'l Conf., BOSS. 1, 659-684.

MORTON, B.R. & TAYLOR, G.I. & TURNER, J.S. 1956 Turbulent gravitational convection from maintained and instantaneous sources. Proc. Roy. Soc. A. 234, 1-23.

SEBAN, R.A. & BEHNIA, M.M. 1976 Turbulent buoyant jets in unstratified surroundings. Int'l J. of Heat Mass Transfer 19, 1197-1204.

SJOEN, K. 1982 Data from measurements in bubble plumes. SINTEF Project Memo. Project #150030 Memo #1.

TOPHAM, D.R. 1975 Hydrodynamics of an oil well blowout. Beaufort Sea Technical Reports, Institute of Ocean Sciences, Sidney, B.C. No.33.

Z	RAW b	RAW U	SMOOTH b	SMOOTH U	q	G	S	GAMMA	N M^3/S AIRFLOW	
1.98	0.162	1.129	0.150	1.127	0.0042	0.077	88.21			
16.47	1.540	0.489	1.572	0.506	0.0055	3.929	1.68	1.24		
25.62	1.920	0.515	1.967	0.477	0.0070	5.797	1.40	1.50		
37.81	2.822	0.498	2.466	0.562	0.0109	10.725	1.28	1.16	0.024	
43.90	2.470	0.608	2.895	0.553	0.0149	14.555	1.29	1.15		
46.95	2.980	0.538	3.191	0.516	0.0184	16.503	1.35	1.26		
1.98	0.250	1.543	0.257	1.542	0.0204	0.306	118.20			
16.47	1.780	0.860	1.732	0.863	0.0272	8.124	5.12	1.23		
25.62	2.399	0.829	2.476	0.823	0.0345	15.834	3.27	1.14	0.118	
37.81	3.686	0.833	3.621	0.838	0.0534	34.475	2.34	0.91		
43.90	4.355	0.745	4.384	0.743	0.0735	44.811	2.36	1.07		
1.98	0.338	1.739	0.328	1.740	0.0490	0.552	159.24			
16.47	2.320	1.114	2.359	1.109	0.0653	19.351	5.65	0.95		
25.62	3.590	0.970	3.583	0.971	0.0827	39.102	3.39	0.83		
37.81	5.569	0.881	5.365	0.906	0.1280	81.840	2.44	0.77	0.283	
43.90	5.976	0.912	6.393	0.861	0.1762	110.426	2.45	0.81		
46.95	7.190	0.794	6.955	0.823	0.2172	124.919	2.62	0.88		
1.98	0.395	2.103	0.412	2.105	0.1022	1.041	182.09			
16.47	2.609	1.326	2.488	1.316	0.1362	25.493	9.44	0.99		
25.62	3.399	1.174	3.615	1.188	0.1723	48.652	6.08	0.99		
37.81	5.556	1.189	5.296	1.184	0.2668	104.145	4.40	0.83	0.590	
43.90	6.108	1.171	6.343	1.162	0.3674	146.677	4.28	0.81		
46.95	7.030	1.121	6.944	1.129	0.4527	170.688	4.49	0.84		BUGG SPRING EXPERIMENT DATA
0.65	0.110	0.985	0.113	0.987	0.0026	0.038	106.55			
2.25	0.300	0.750	0.293	0.748	0.0028	0.200	20.41	1.06		
3.85	0.465	0.630	0.465	0.620	0.0031	0.420	9.83	1.08		
5.45	0.600	0.545	0.614	0.569	0.0035	0.672	6.55	1.11	0.005	
7.05	0.735	0.585	0.721	0.586	0.0039	0.922	5.35	1.13		
8.65	0.765	0.575	0.769	0.580	0.0044	1.076	5.30	1.25		
0.65	0.135	0.975	0.134	0.978	0.0052	0.052	152.73			
2.25	0.310	0.900	0.307	0.893	0.0057	0.260	33.51	1.30		
3.85	0.465	0.815	0.491	0.815	0.0062	0.614	15.18	1.03		
5.45	0.710	0.735	0.685	0.749	0.0069	1.036	9.65	0.99	0.010	
7.05	0.775	0.710	0.807	0.696	0.0078	1.420	7.67	1.07		
8.65	0.905	0.655	0.897	0.659	0.0089	1.860	7.31	1.28		
0.65	0.135	1.130	0.134	1.131	0.0078	0.059	206.48			
2.25	0.355	1.050	0.362	1.049	0.0085	0.426	32.63	0.91		
3.85	0.540	0.975	0.518	0.974	0.0094	0.816	18.33	0.88		
5.45	0.615	0.900	0.645	0.904	0.0104	1.174	13.79	0.97	0.015	
7.05	0.800	0.840	0.781	0.836	0.0117	1.596	11.06	1.07		
8.65	0.965	0.765	0.970	0.766	0.0133	2.255	8.63	1.08		
0.65	0.155	1.170	0.161	1.162	0.0115	0.086	209.19			
2.25	0.350	1.055	0.334	1.077	0.0126	0.369	55.53	1.47		
3.85	0.515	1.020	0.524	1.008	0.0138	0.860	25.88	1.15		
5.45	0.705	0.965	0.720	0.945	0.0153	1.529	15.85	1.02	0.0221	
7.05	0.930	0.855	0.911	0.881	0.0172	2.286	11.62	1.01		
8.65	1.080	0.815	1.086	0.807	0.0197	2.978	9.83	1.13		FANNELOP AND SJOEN DATA
0.32	0.025	0.862	0.024	0.864	0.0002	0.001	168.73			
0.96	0.063	0.438	0.064	0.432	0.0002	0.006	31.50	2.10		
1.58	0.103	0.321	0.101	0.331	0.0002	0.011	15.03	2.45	0.00021	
2.20	0.128	0.326	0.129	0.319	0.0002	0.017	9.76	2.32		
2.78	0.144	0.358	0.144	0.360	0.0002	0.023	7.95	1.93		
0.32	0.031	0.774	0.030	0.772	0.0004	0.002	244.43			
0.96	0.082	0.527	0.085	0.537	0.0004	0.012	40.01	1.74		
1.58	0.129	0.456	0.125	0.441	0.0004	0.021	21.40	2.00	0.00050	
2.20	0.158	0.418	0.161	0.426	0.0004	0.034	13.72	1.85		
2.78	0.201	0.445	0.200	0.442	0.0005	0.056	9.17	1.44		
0.32	0.039	0.903	0.039	0.896	0.0009	0.004	312.58			
0.96	0.100	0.598	0.099	0.628	0.0009	0.019	63.62	2.02		
1.58	0.137	0.553	0.138	0.507	0.0010	0.030	38.18	2.66	0.00118	
2.20	0.183	0.446	0.182	0.478	0.0010	0.049	23.83	2.51		
2.78	0.248	0.498	0.248	0.490	0.0011	0.094	13.41	1.89		
0.32	0.048	1.021	0.048	1.017	0.0018	0.006	387.81			
0.96	0.117	0.675	0.116	0.691	0.0018	0.028	87.76	2.28		
1.58	0.167	0.594	0.168	0.569	0.0019	0.050	48.91	2.70	0.00234	
2.20	0.223	0.539	0.222	0.556	0.0020	0.085	29.94	2.35		
2.78	0.288	0.580	0.288	0.575	0.0022	0.149	18.43	1.70		MILGRAM AND VAN HOUTEN DATA

TABLE 1. The Momentum Amplification Factors and Plume Properties Obtained from the Data Analysis at the Measurement Heights.

Z	b	U	q	S	W	ALPHA	N M^3/S AIRFLOW	
9.23	0.86	0.817	0.0047	44.95	0.290	0.060		
21.05	1.77	0.492	0.0062	1.54	0.183	0.037		
31.71	2.22	0.520	0.0085	1.34	0.244	0.056	0.024	
40.86	2.68	0.557	0.0126	1.28	0.122	0.067		
45.43	3.04	0.535	0.0165	1.32	0.061	0.063		
9.23	0.99	1.203	0.0234	61.66	0.290	0.072		
21.05	2.10	0.843	0.0304	4.19	0.183	0.076	0.118	
31.71	3.05	0.831	0.0419	2.81	0.244	0.096		
40.86	4.00	0.790	0.0618	2.35	0.122	0.085		
9.23	1.34	1.425	0.0560	82.45	0.290	0.108		
21.05	2.87	1.040	0.0730	4.52	0.183	0.111		
31.71	4.47	0.938	0.1004	2.91	0.244	0.133	0.283	
40.86	5.88	0.883	0.1483	2.44	0.122	0.144		
45.43	6.67	0.842	0.1946	2.53	0.061	0.135		
9.23	1.45	1.710	0.1168	95.77	0.290	0.108		
21.05	3.05	1.252	0.1521	7.76	0.183	0.106		
31.71	4.46	1.186	0.2094	5.24	0.244	0.137	0.590	
40.86	5.82	1.173	0.3091	4.34	0.122	0.163		
45.43	6.64	1.146	0.4056	4.39	0.061	0.165		BUGG SPRING EXPERIMENT DATA
1.45	0.20	0.868	0.0027	63.48	0.162	0.092		
3.05	0.38	0.884	0.0030	15.12	0.162	0.084		
4.65	0.54	0.594	0.0033	8.19	0.162	0.078	0.005	
6.25	0.67	0.568	0.0037	5.95	0.162	0.066		
7.85	0.75	0.573	0.0041	5.33	0.162	0.036		
1.45	0.22	0.935	0.0054	93.12	0.162	0.101		
3.05	0.40	0.854	0.0060	24.34	0.162	0.103		
4.65	0.58	0.782	0.0066	12.42	0.162	0.093	0.010	
6.25	0.74	0.722	0.0073	8.66	0.162	0.072		
7.85	0.85	0.678	0.0083	7.49	0.162	0.041		
1.45	0.25	1.090	0.0082	119.56	0.162	0.135		
3.05	0.44	1.011	0.0089	25.48	0.162	0.087		
4.65	0.58	0.939	0.0099	16.06	0.162	0.065	0.015	
6.25	0.71	0.870	0.0110	12.42	0.162	0.068		
7.85	0.88	0.801	0.0125	9.84	0.162	0.093		
1.45	0.25	1.120	0.0120	132.36	0.162	0.102		
3.05	0.43	1.042	0.0131	40.71	0.162	0.109		
4.65	0.62	0.976	0.0145	20.87	0.162	0.110	0.0221	
6.25	0.82	0.913	0.0162	13.73	0.162	0.101		
7.85	1.00	0.844	0.0184	10.72	0.162	0.082		FANNELOP AND SJOEN DATA
0.64	0.04	0.548	0.0002	100.11	0.175	0.045		
1.27	0.08	0.381	0.0002	23.27	0.169	0.040	0.00021	
1.89	0.12	0.325	0.0002	12.39	0.169	0.043		
2.49	0.14	0.340	0.0002	8.85	0.158	0.039		
0.64	0.06	0.654	0.0004	142.22	0.175	0.065		
1.27	0.10	0.489	0.0004	30.70	0.169	0.047	0.00050	
1.89	0.14	0.434	0.0004	17.56	0.169	0.055		
2.49	0.18	0.434	0.0004	11.44	0.158	0.074		
0.64	0.07	0.762	0.0009	188.10	0.175	0.071		
1.27	0.12	0.568	0.0010	50.90	0.169	0.042	0.00118	
1.89	0.16	0.493	0.0010	31.01	0.169	0.063		
2.49	0.22	0.484	0.0011	18.62	0.158	0.118		
0.64	0.08	0.854	0.0018	237.78	0.175	0.078		
1.27	0.14	0.630	0.0019	68.33	0.169	0.060	0.00234	
1.89	0.19	0.563	0.0020	39.43	0.169	0.083		
2.49	0.25	0.566	0.0021	24.19	0.158	0.121		MILGRAM AND VAN HOUTEN DATA

TABLE 2. The Entrainment Coefficients and Plume Properties at Heights Midway Between Measurement Heights.

The entrainment coefficients have been evaluated by equation (2.25) and the properties b, U, q and S are the averages of the values above and below the midpoints. W is the distance $z_{i=1}-z_i$ used in equation (2.25) divided by the total plume height.

	----RAW-----		---SMOOTH---						N M3/S		
Z	b	U	b	U	q	Q	S	GAMMA	AIRFLOW		
0.71	0.078	0.380	0.079	0.388	0.0003	0.007	39.88				
1.00	0.102	0.380	0.100	0.385	0.0003	0.012	25.08	2.78			
1.50	0.127	0.380	0.130	0.376	0.0003	0.020	15.61	2.40			
2.23	0.173	0.370	0.167	0.367	0.0003	0.032	10.09	2.19	0.00040		
2.78	0.192	0.350	0.200	0.369	0.0003	0.046	7.40	1.89			
3.22	0.233	0.400	0.228	0.373	0.0004	0.061	5.86	1.64			
3.76	0.260	0.350	0.261	0.371	0.0004	0.079	4.72	1.50			
4.05	0.276	0.370	0.276	0.361	0.0004	0.086	4.38	1.53			
0.71	0.088	0.530	0.088	0.530	0.0004	0.013	39.53				
1.00	0.110	0.530	0.110	0.533	0.0004	0.020	25.77	1.43			
1.50	0.143	0.520	0.144	0.509	0.0004	0.033	15.86	1.28			
2.23	0.192	0.440	0.189	0.463	0.0005	0.052	10.21	1.31	0.00057		KOBUS DATA
2.78	0.219	0.490	0.221	0.466	0.0005	0.071	7.79	1.19			
3.22	0.247	0.480	0.248	0.484	0.0005	0.093	6.33	1.03			
3.76	0.287	0.470	0.285	0.478	0.0005	0.122	5.07	0.94			
4.15	0.315	0.430	0.316	0.426	0.0006	0.133	4.50	1.08			
5.00	1.591	1.209	1.674	1.238	0.0567	10.859	9.04				
14.00	3.383	1.466	3.067	1.375	0.0659	40.599	2.91	0.32			
23.00	4.013	1.191	4.444	1.266	0.0785	78.520	1.75	0.29	0.367		
32.00	5.657	1.110	5.430	1.141	0.0970	105.609	1.56	0.36			
42.00	5.606	1.350	5.609	1.262	0.1316	124.681	1.85	0.40			
48.00	5.022	1.550	5.048	1.593	0.1674	127.421	2.47	0.38			
5.00	1.518	1.432	1.544	1.438	0.0685	10.724	11.55				
15.00	2.168	1.544	2.053	1.517	0.0809	20.036	7.44	0.84			
24.00	2.718	1.148	2.888	1.187	0.0968	31.050	5.34	0.89	0.443		
34.00	4.228	0.904	4.115	0.878	0.1236	46.606	4.08	1.35			
42.70	5.307	1.061	5.339	1.068	0.1629	95.572	2.93	0.79			
4.50	1.232	1.149	1.191	1.226	0.1134	5.388	35.93				
7.60	1.448	1.617	1.520	1.501	0.1197	10.814	20.21	1.23			
17.00	3.012	1.545	2.948	1.570	0.1442	42.767	6.27	0.55	0.560		
26.00	4.414	1.026	4.467	1.116	0.1792	69.827	4.31	0.80			
32.00	5.303	0.972	5.281	0.877	0.2138	76.660	4.29	1.29			
42.00	5.770	1.201	5.771	1.221	0.3153	127.530	4.29	0.89			TOPHAM DATA

TABLE 3. The Momentum Amplification Factora and Plume Properties Obtained for the Kobus and Topham Data from Data Analysis at the Measurement Heights.

Z	b	U	q	S	W	ALPHA	N M^3/S AIRFLOW	
0.86	0.09	0.386	0.0003	32.47	0.064	0.074		KOBUS DATA
1.25	0.12	0.381	0.0003	20.34	0.111	0.057		
1.86	0.15	0.372	0.0003	12.85	0.162	0.048		
2.51	0.18	0.368	0.0003	8.74	0.122	0.060	0.00040	
3.00	0.21	0.371	0.0004	6.63	0.098	0.057		
3.49	0.24	0.372	0.0004	5.29	0.120	0.059		
3.90	0.27	0.366	0.0004	4.55	0.064	0.040		
0.86	0.10	0.531	0.0004	32.65	0.064	0.077		
1.25	0.13	0.521	0.0004	20.82	0.111	0.063		
1.86	0.17	0.488	0.0004	13.04	0.162	0.050		
2.51	0.21	0.465	0.0005	9.00	0.122	0.060	0.00057	
3.00	0.23	0.475	0.0005	7.06	0.098	0.071		
3.48	0.27	0.481	0.0005	5.70	0.120	0.065		
3.95	0.30	0.452	0.0005	4.78	0.087	0.035		
9.50	2.37	1.307	0.0610	5.97	0.150	0.170		TOPHAM DATA
18.50	3.76	1.321	0.0716	2.33	0.150	0.135		
27.50	4.94	1.204	0.0867	1.65	0.150	0.081	0.367	
37.00	5.52	1.202	0.1117	1.70	0.167	0.046		
45.00	5.33	1.428	0.1473	2.16	0.100	0.010		
10.00	1.80	1.478	0.0742	9.49	0.167	0.056		
19.50	2.47	1.352	0.0881	6.39	0.150	0.058	0.443	
29.00	3.50	1.033	0.1085	4.71	0.167	0.069		
38.35	4.73	0.973	0.1405	3.46	0.145	0.195		
6.05	1.36	1.364	0.1165	28.07	0.058	0.151		
12.30	2.23	1.535	0.1308	13.24	0.177	0.158		
21.50	3.71	1.343	0.1598	5.29	0.170	0.096	0.660	
29.00	4.87	0.996	0.1949	4.30	0.113	0.037		
37.00	5.53	1.049	0.2548	4.29	0.189	0.140		

TABLE 4. The Entrainment Coefficients and Plume Properties at Heights Midway Between Measurement Heights for the Kobus and Topham Data.

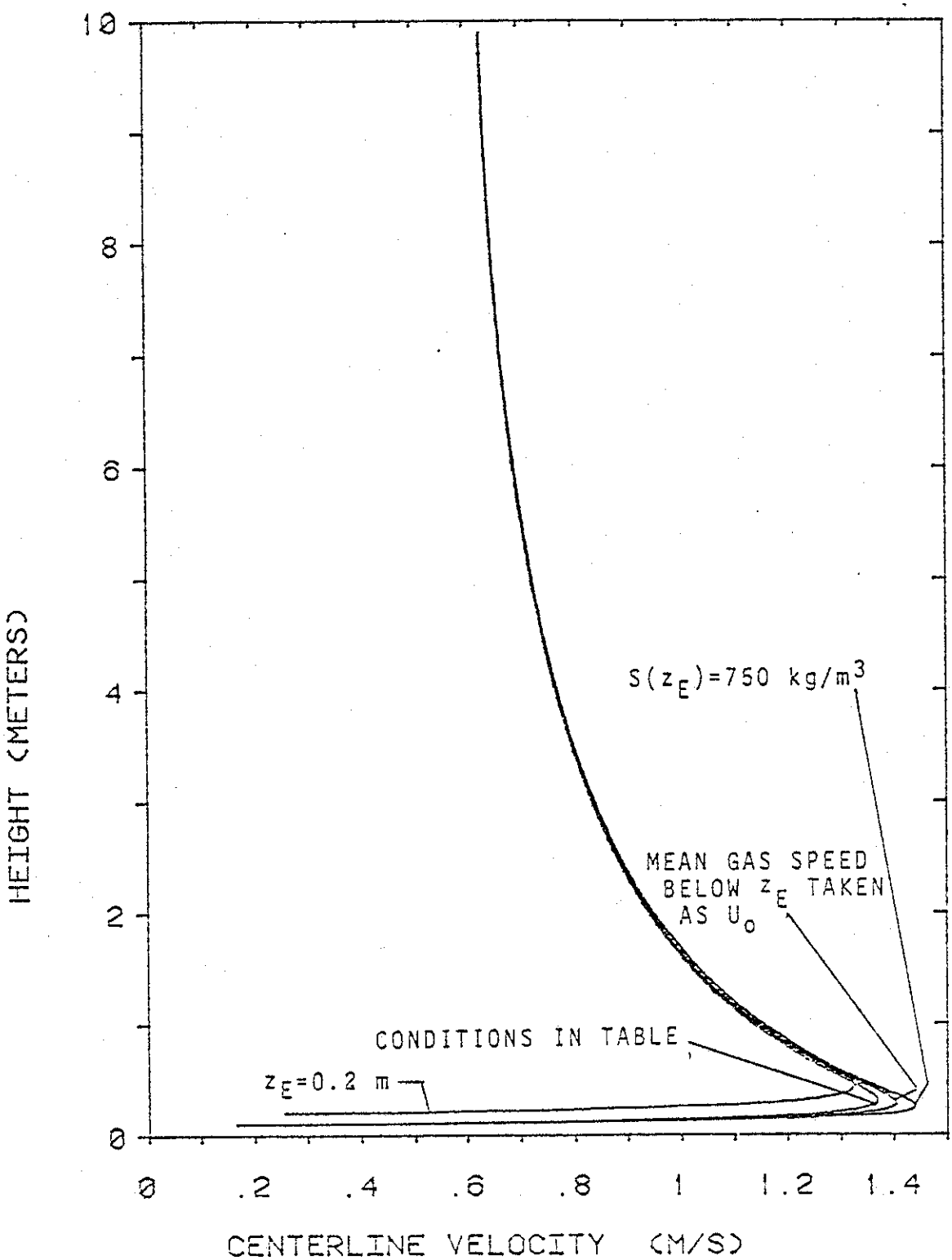

FIGURE 2.1 The Effect of Variations in Initial Conditions for Starting the Numerical Integrations

Conditions are as listed below except for notations on individual curves.

$H=10$ m $\quad Z_E=0.1$ m $\quad g=9.81$ m^2/s $\quad q=0.01$ N m^3/s $\quad S(z_E)=500$ Kg/m^3

$u_o=25$ m/s $\quad \rho_T=1.3$ Kg/m^3 $\quad \rho_w=1000$ kg/m^3 $\quad \lambda=0.8$ $\quad \gamma=1.5$ $\quad \alpha=0.08$

$u_b=0.35$ m/s . Mean gas speed below Z_E taken as $u_o/2$

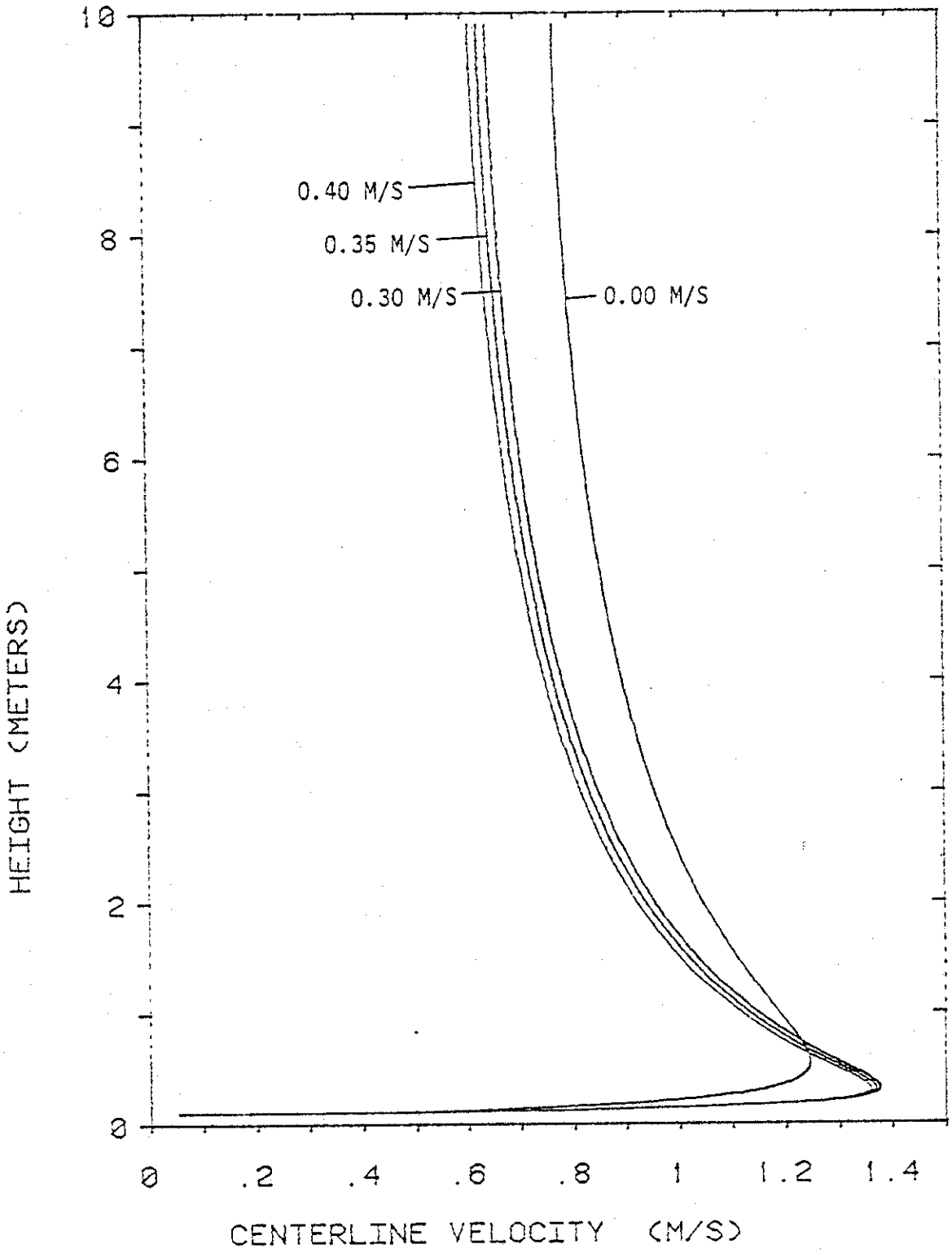

FIGURE 2.2 Effect of Gas Bubble Slip Speed on Solution to the Plume Equations
The bubble slip speeds used in the calculations are shown on each curve. Other conditions are as given in figure 2.1.

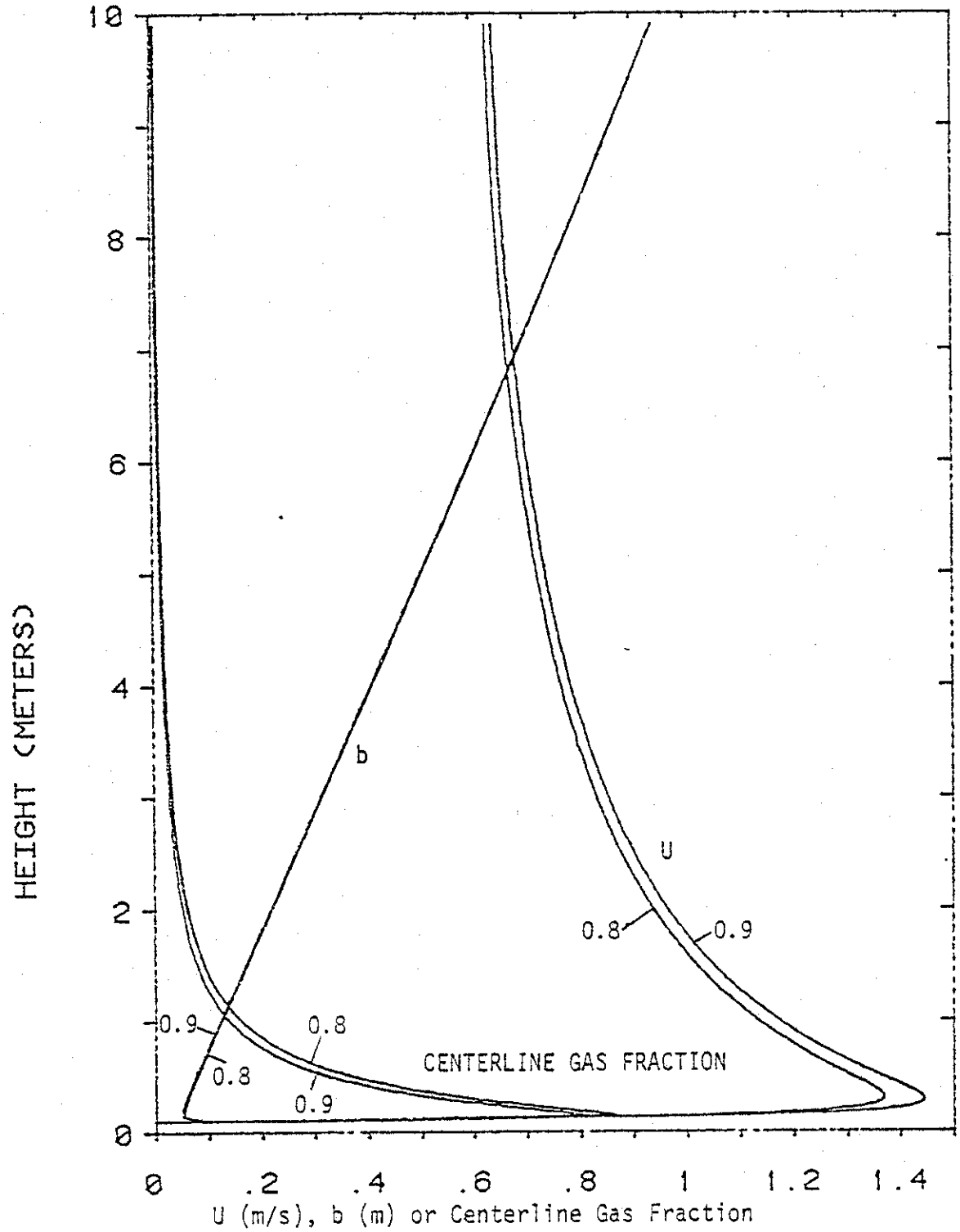

FIGURE 2.3 Numerical Results for Gas-Velocity Radius Ratios, λ, of 0.8 and 0.9
The conditions for the calculations are those given in figure 2.1.
The values for λ are shown on the curves.
The difference in plume radius, b, for the two values of λ is almost undiscernable.

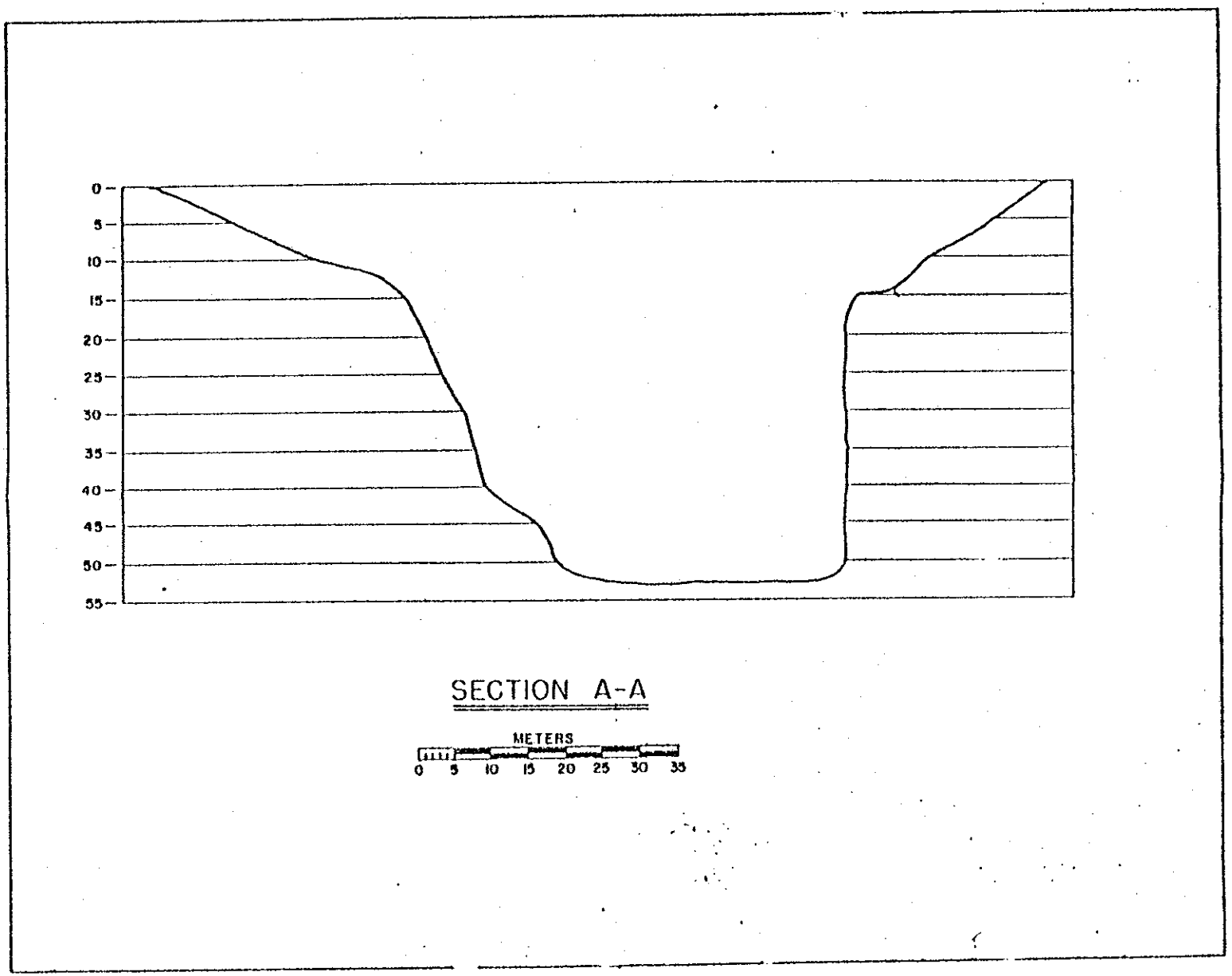

FIGURE 3.1 A Depth Profile of Bugg Spring

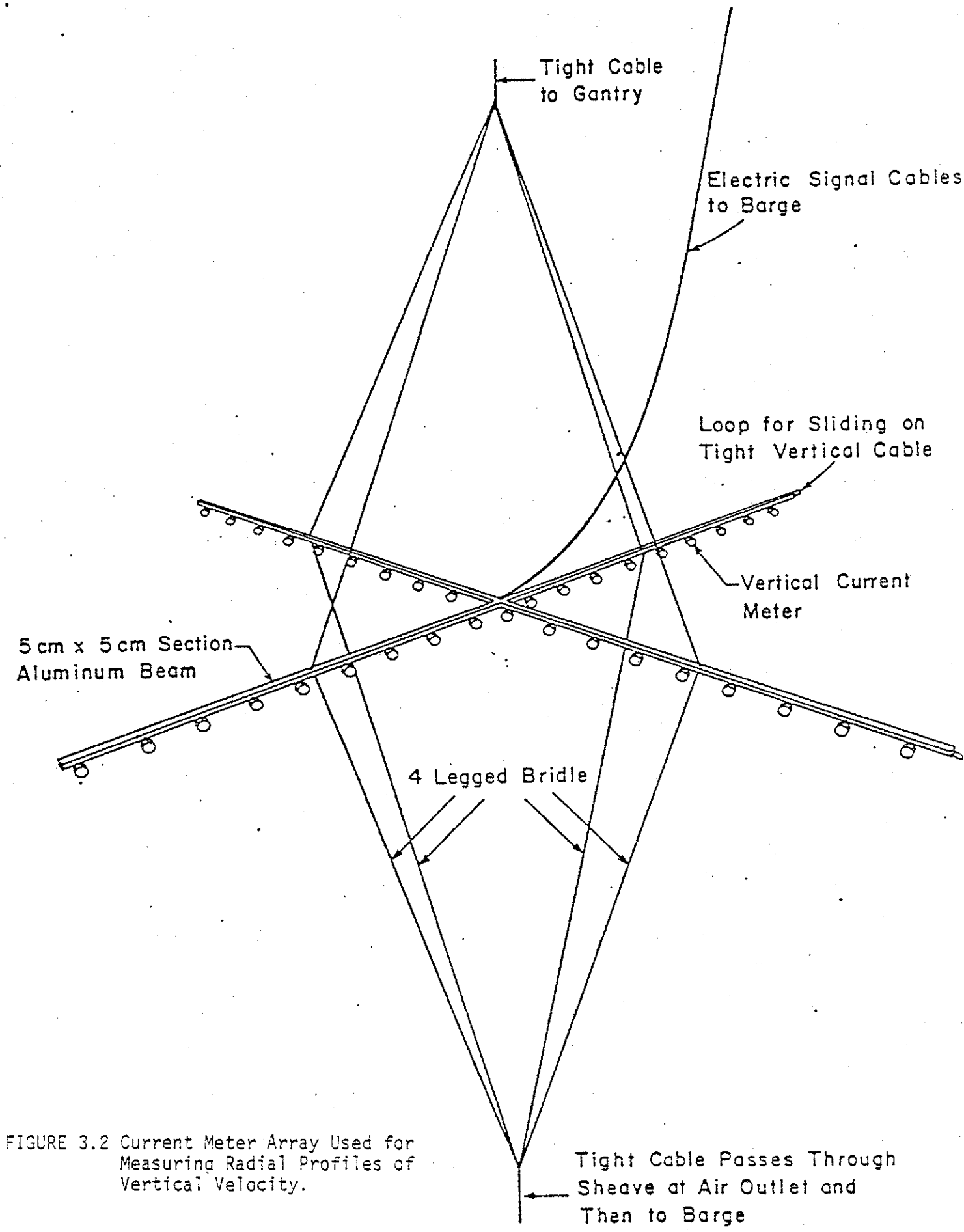

FIGURE 3.2 Current Meter Array Used for Measuring Radial Profiles of Vertical Velocity.

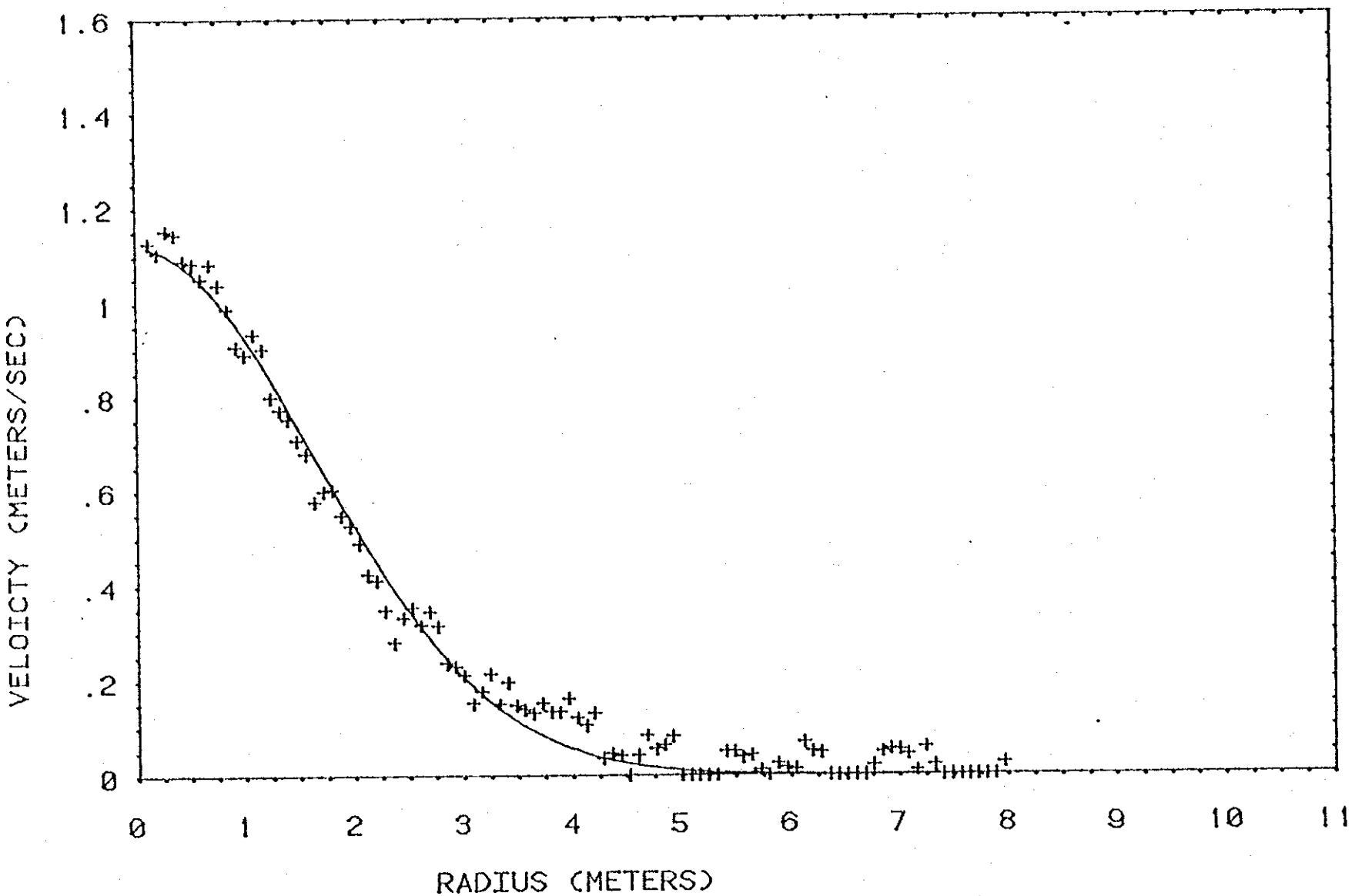

FIGURE 3.3 An Example of Reduced Data for a Radial Profile of Vertical Velocity

The case shown is for a gas flow rate of 0.283 N m^3/s and a height of 16.47 m above the gas outlet.

\+ reduced data point ——————— Gaussian function fit to the data

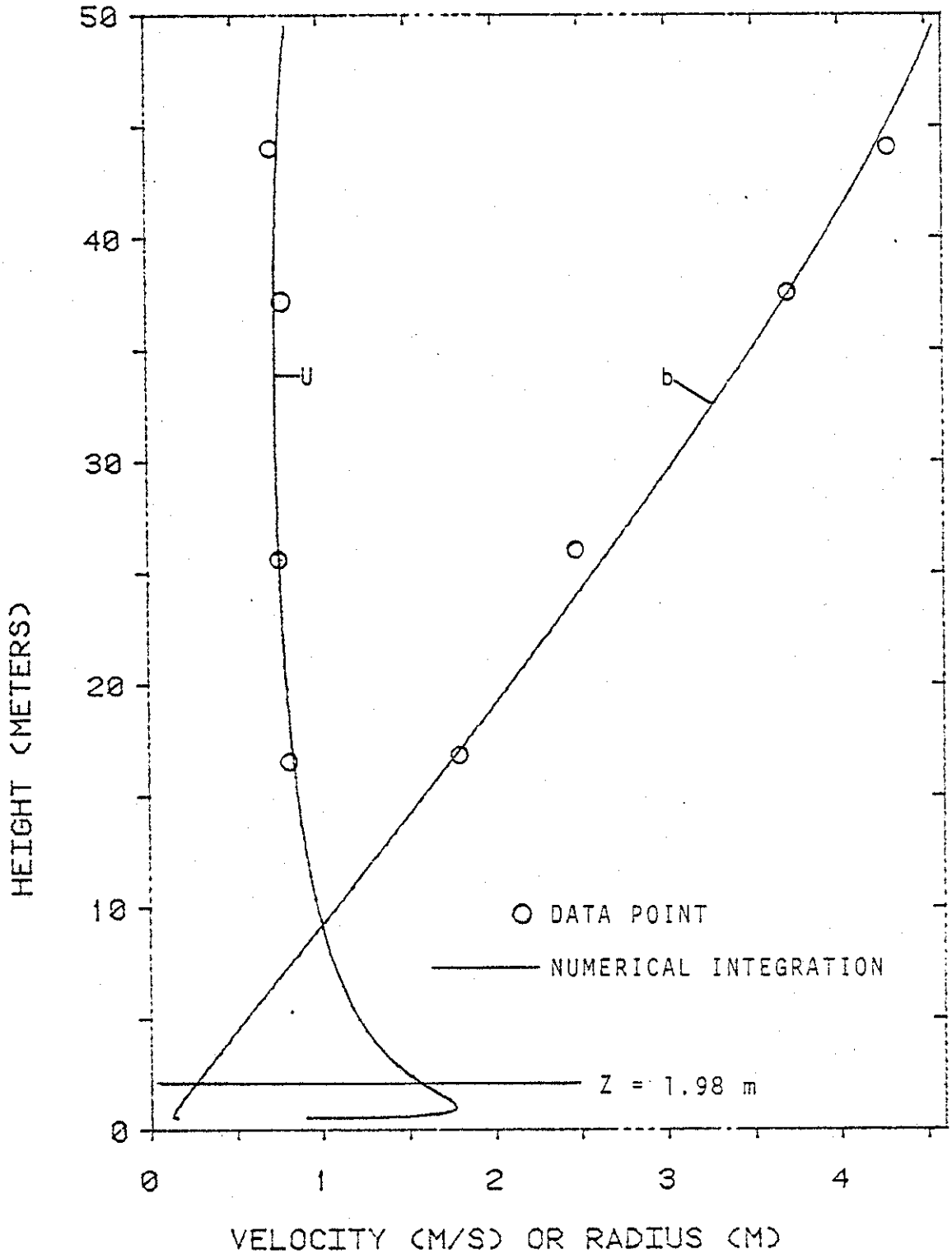

FIGURE 4.1 Example of a Numerical Integration Used to Estimate Conditions at a Low Point in the Zone of Established Flow

The conditions of the example correspond to an airflow rate of 0.118 N m^3/s in the Bugg Spring Experiments. The numerical integration was done with λ=0.8, Z_E=0.5 m and $S(z_E)$=500 kg/m^3. The best fit to the data was with γ=1.1 and α=0.087 which is the case that is shown.

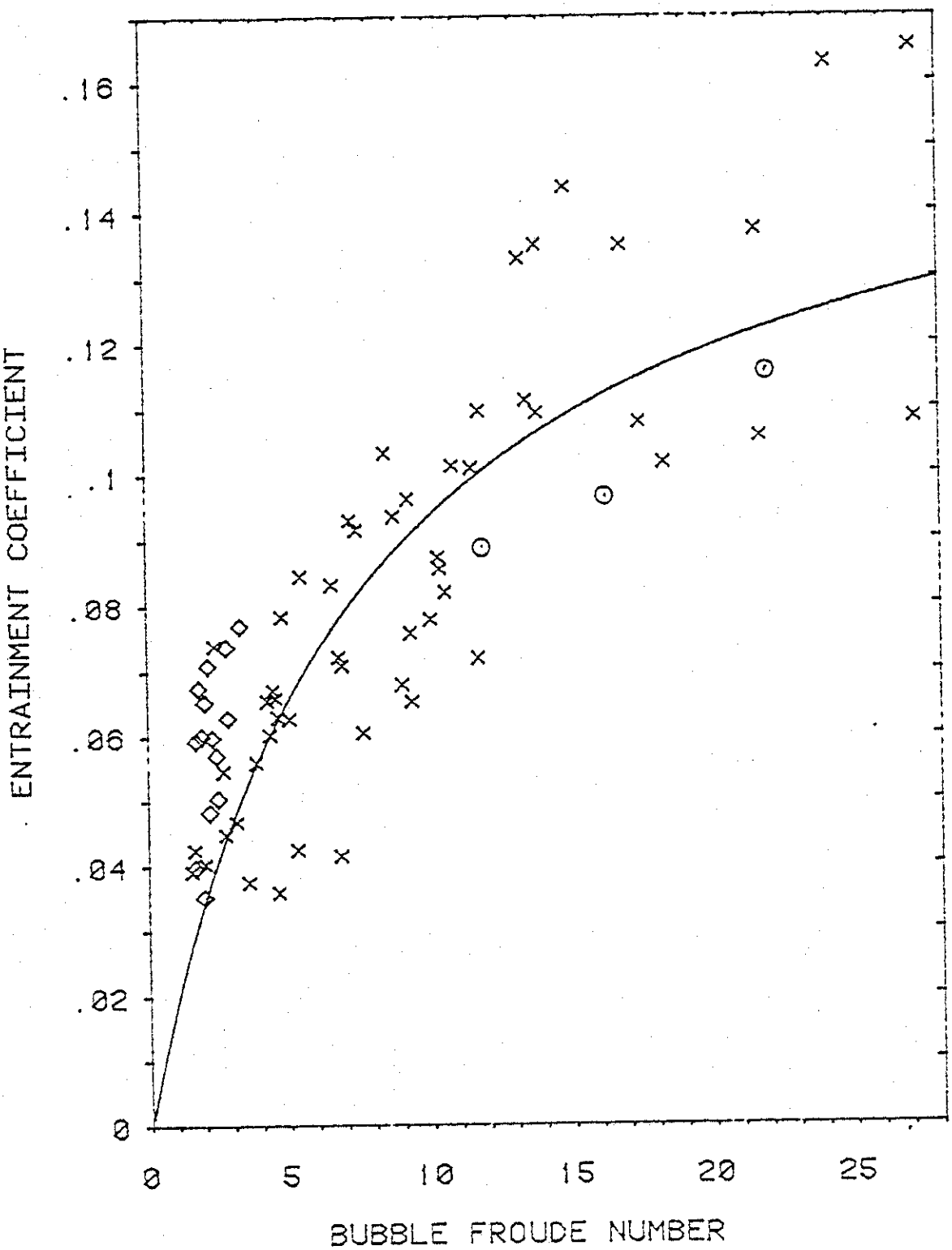

FIGURE 4.2 The Entrainment Coefficient, α, Vs The Bubble Froude Number, F_B

× - Calculated from primary data set

◇ - Calculated from subsonic orifice Kobus data

○ - Average of Calculated values from Topham data. The points shown, from left to right are for gas outlet depths of 60, 60 and 53 meters and gas flow rates of 0.367, 0.443 and 0.660 N m^3/S respectively

——— Equation (4.9) with K =0.165 and A=7.598

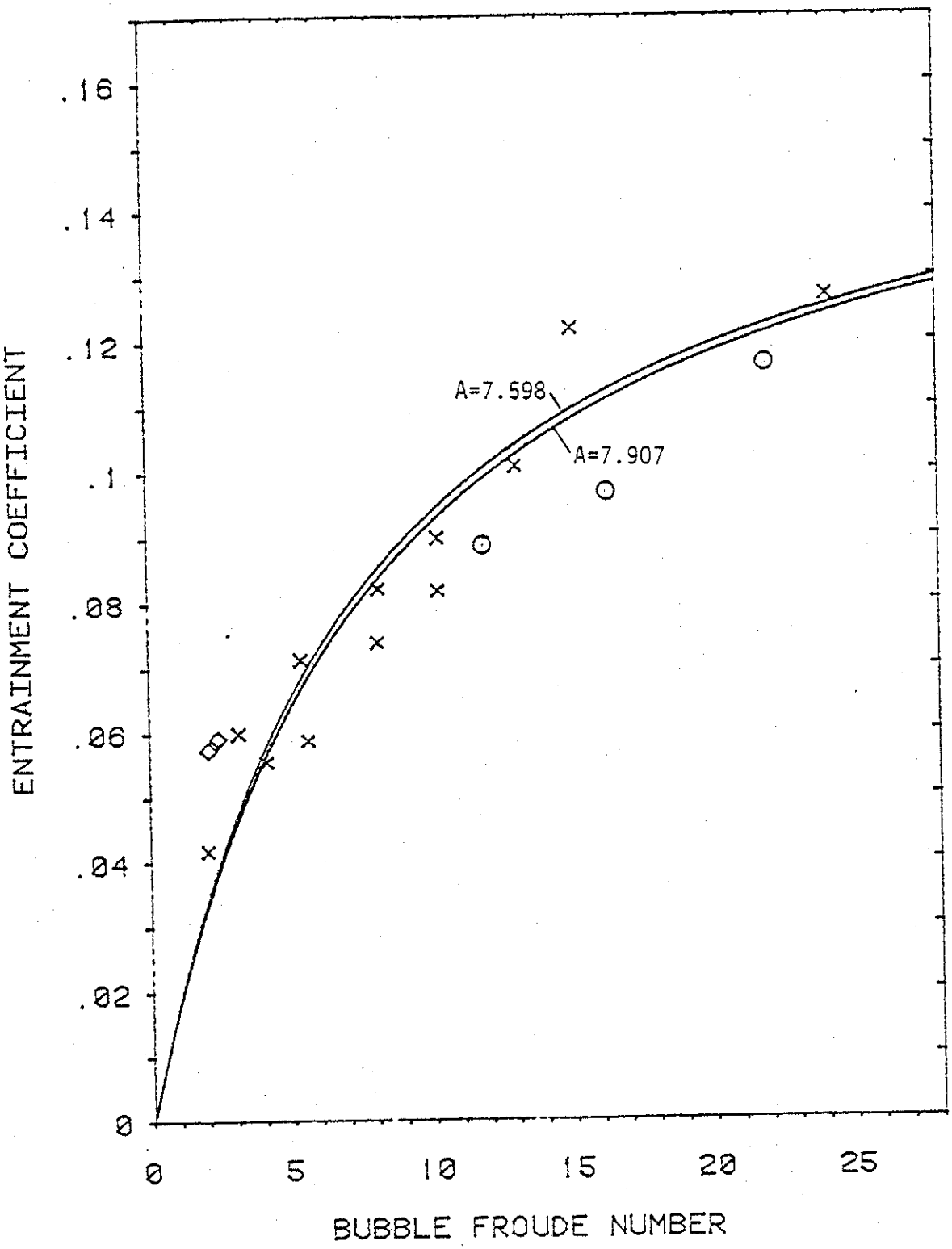

FIGURE 4.3 Entrainment Coefficent Vs Bubble Froude Number for Height-Averaged Data

× - Calculated from primary data set

◇ - Calculated from subsonic orifice Kobus data

○ - Calculated from Topham Data

——— Equation (4.9) with K = 0.165 and A as shown

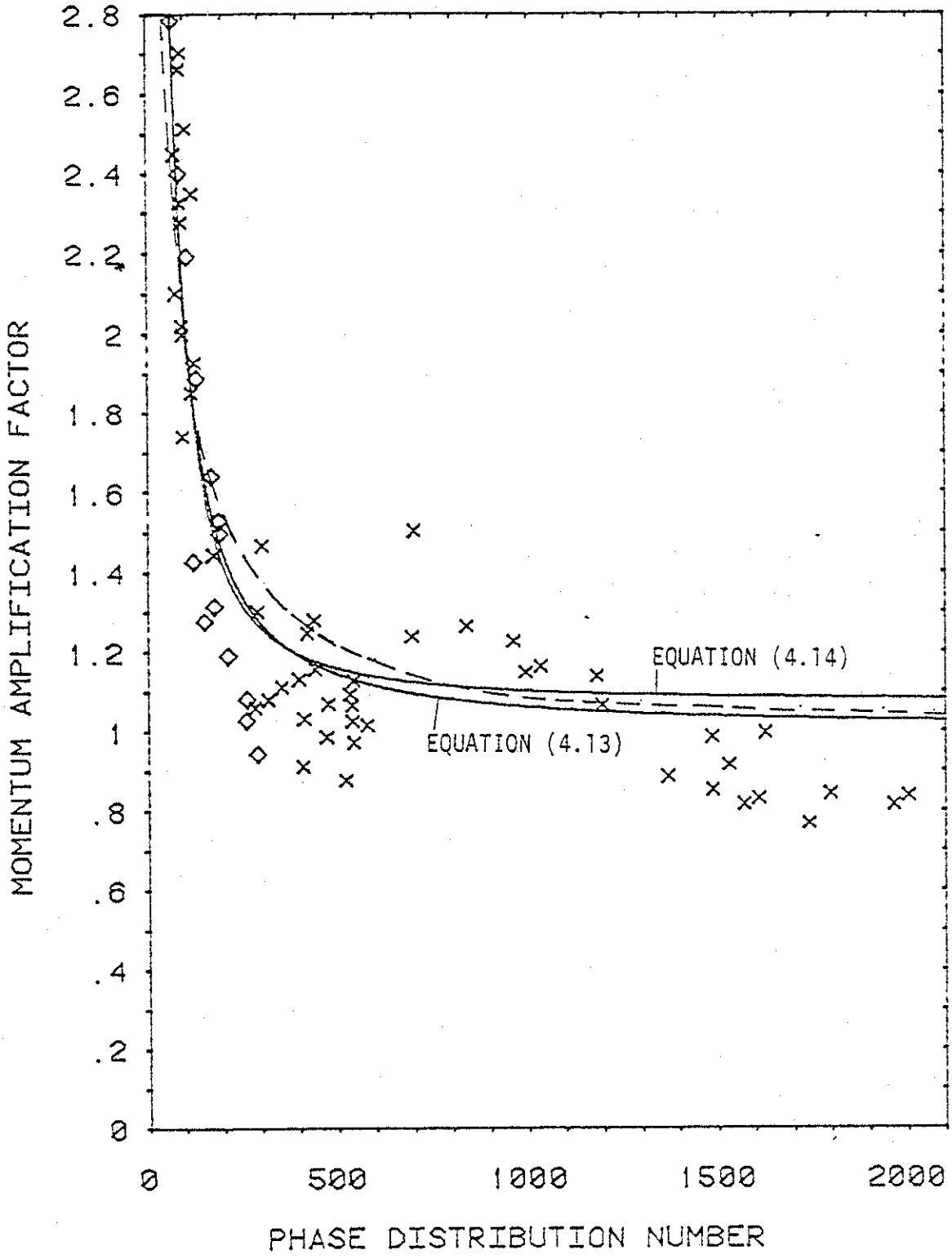

FIGURE 4.4 The Momentum Amplification Factor, γ, Vs the Phase Distribution Number, N_p

× - Calculated from primary data set

◇ - Calculated from subsonic orifice Kobus data

——— Equation (4.13) with C_1=377.7 and C_2=1.25, and Equation (4.14) with D_1=977 and D_2=1.5

— — — — — Equation (4.13) with C_1 =111.3 and C_2 = 1.0

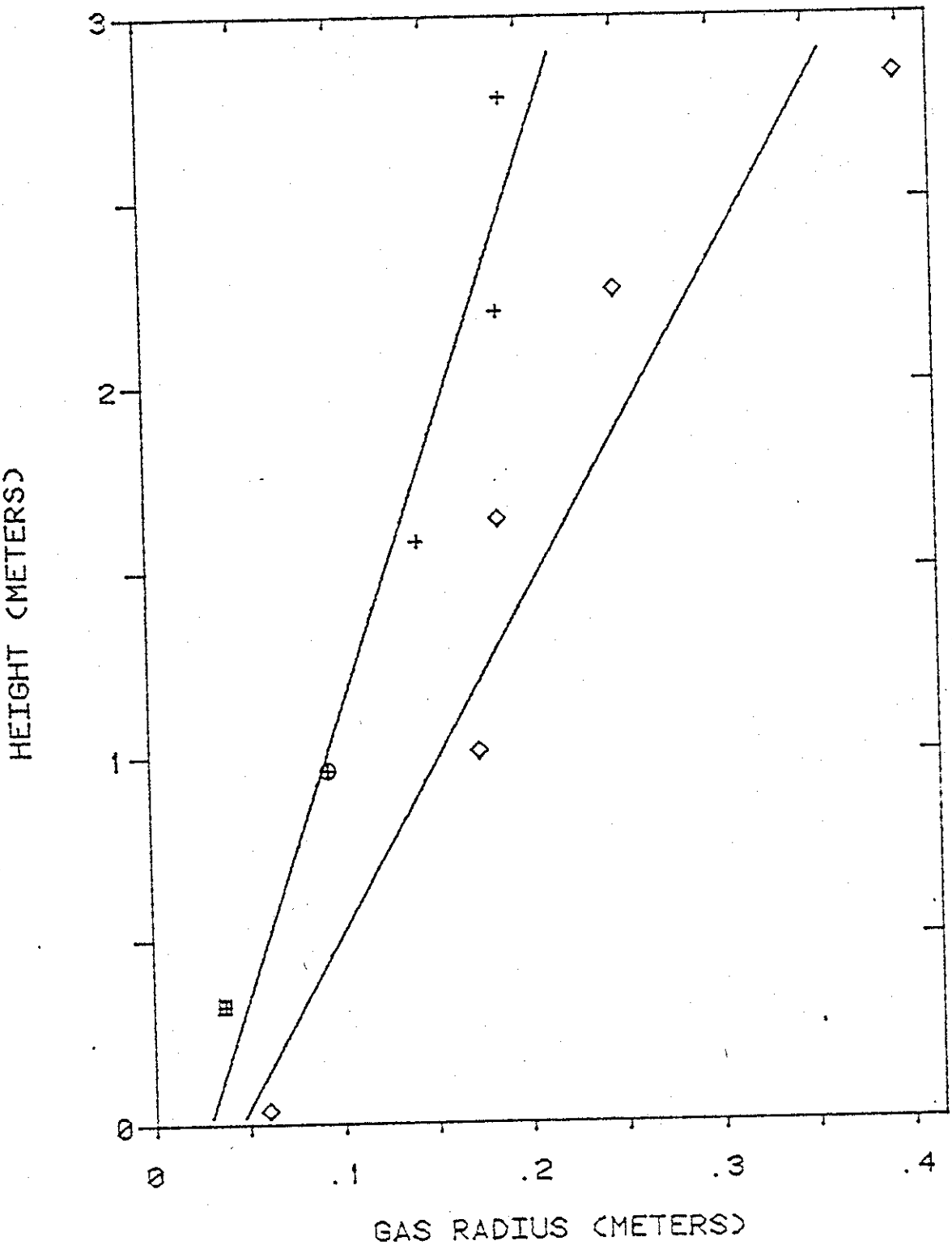

FIGURE 5.1 GAS RADIUS, λb, VS HEIGHT FOR SMALL SCALE PLUMES

◇ Long-term time average measurements of Fazal
\+ Measurements of Milgram and Van Houten relative to instantaneous centerline
⊕ 0.8 x b (from velocity data) for above
⊞ 0.8 x calculated value of b at z_B for above
Best straight line fits to data (minimum mean square error)

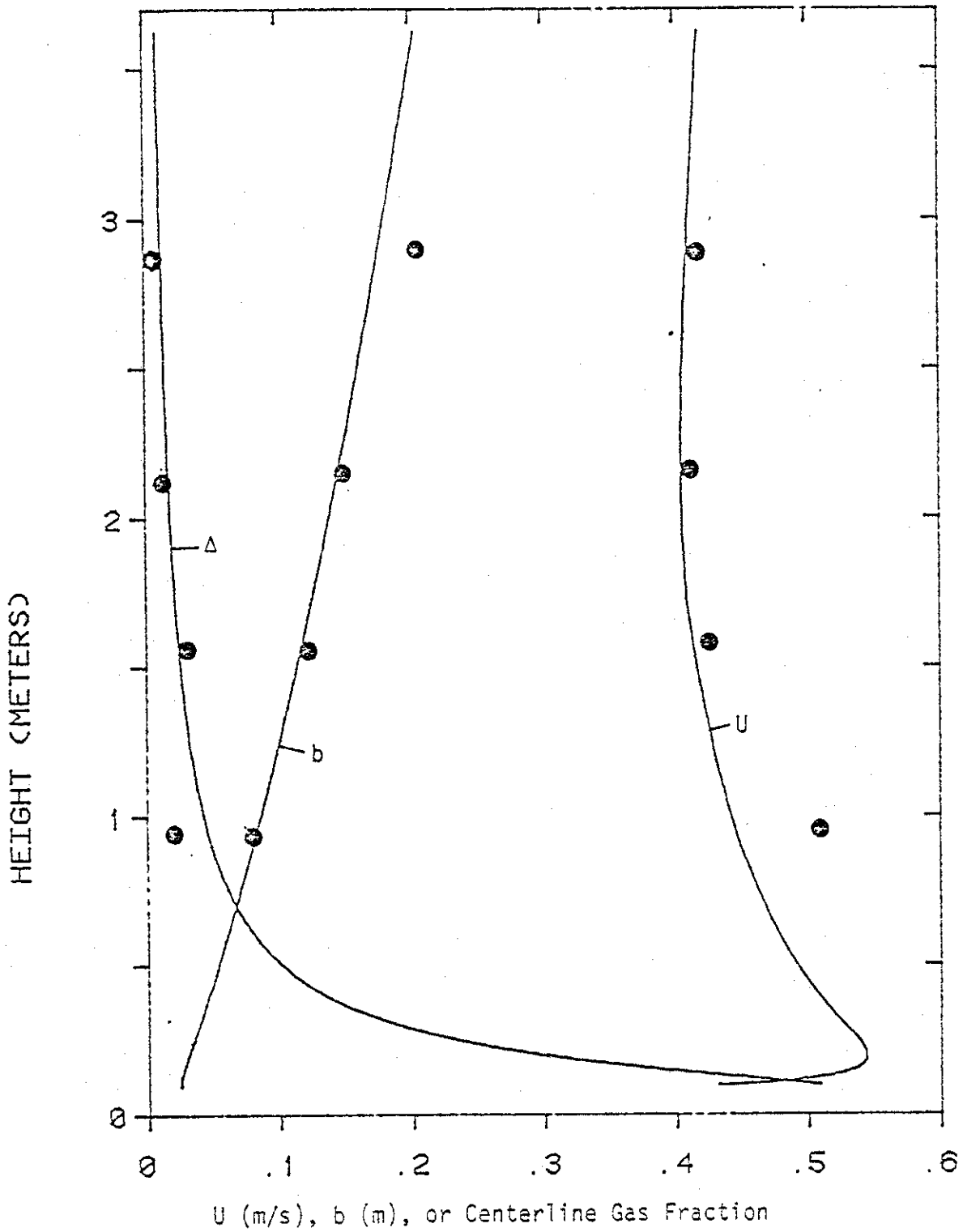

FIGURE 6.1 Application of the Theory to the Experimental Conditions of Milgram and Van Houten at a Gas Flow Rate of 0.00050 N m^3/s

——— Numerical solution from the Theory

○ Experimental Value

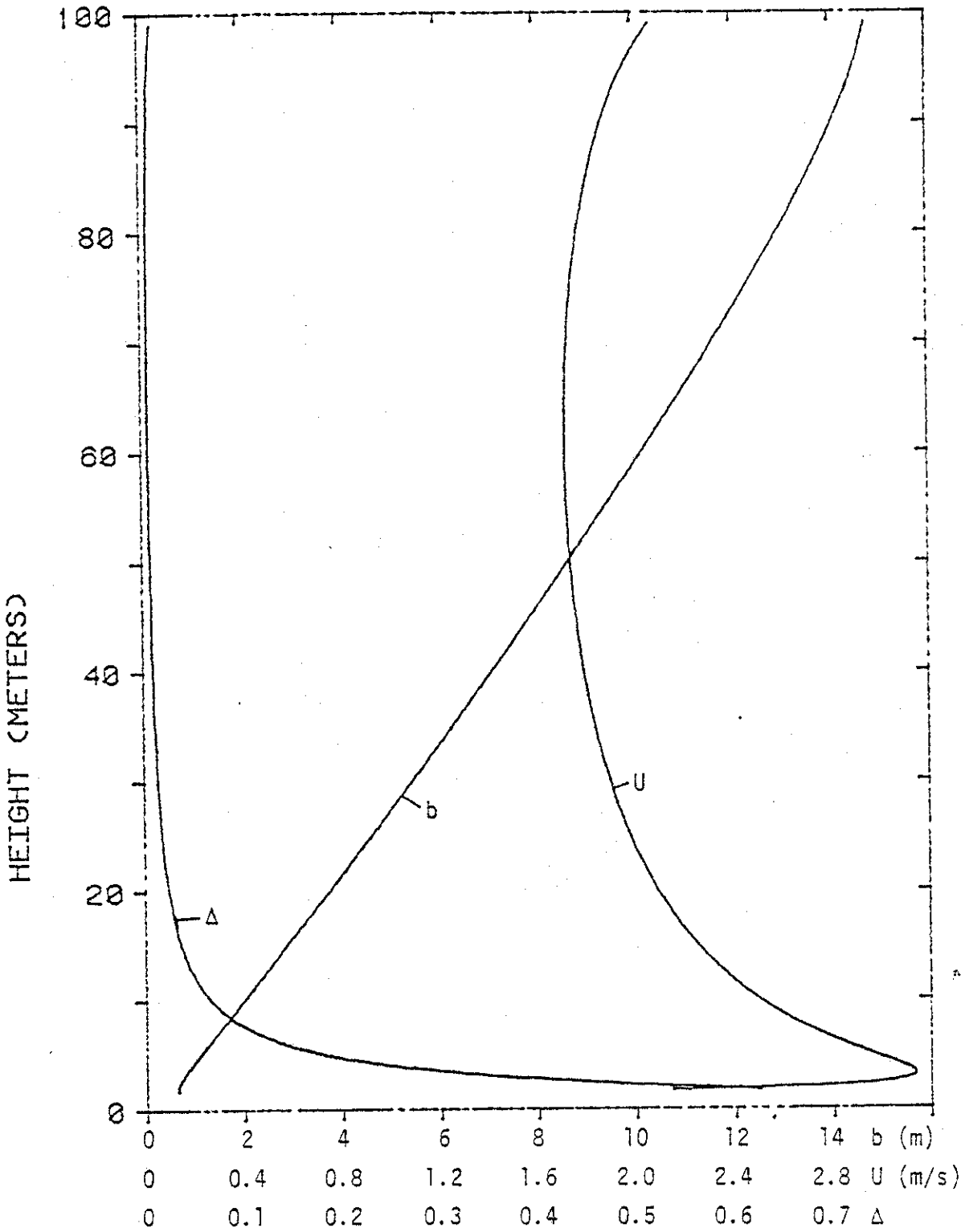

FIGURE 6.2 Results of Numerical Integration of the Plume Equations for a Gas Flow Rate of 10 N m^3/s in Water that is 100 Meters Deep